Seasonal and sub-seasonal rainfall and river flow prediction for Northern Ethiopia

Ph.D. research proposal

Alem Tadesse Haile

Supervisory Committee:

Dr.ir. Chris Mannaerts	(promoter)	ITC, University of Twente,
Dr. B.H.P. Maathuis	(co-promoter)	ITC, University of Twente
Dr. Amanuel Zenebe	(co-promoter)	Mekelle University, Ethiopia

ITC
UNIVERSITY
OF TWENTE.

Table of Contents

Abstract

Reliable weather and climate predictions at sub-seasonal-to-seasonal timescales have significant societal and economic impacts. This can be possible mainly by investigating the interaction among the atmosphere, land surface and the slowly varying ocean surfaces temperature. In Ethiopia, in general, the weather and climate prediction skills are very low and unreliable. Besides, catchment level hydrometeorological responses at seasonal and sub-seasonal temporal scale are not well investigated. Dependence on such weak predictions and exposure to climate risk characterize the livelihoods of substantial parts of Ethiopia's population; and frustrate efforts to sustainably intensify agricultural production, reduce poverty and enhance food security. Though there are few studies that have shown statistical associations among the Ethiopian JJAS rainfall, remotely SST anomalies and regional (local) atmospheric circulation, the prediction skills are inconsistent both spatially and temporally. This might be due to the fact that the Northern Ethiopian climate system is complicated because of numerous climate driving factors interaction and complex topography. In such a region, the interaction and topographic complicity can be better understood by employing either hybrid models (by combining statistical with numerical models) or coupled numerical models such as coupling the ocean with the atmosphere and/or the atmosphere with the terrestrial system. This research is, therefore, set-out to improve the prediction skill of the main rainy season (JJAS) and river flow with a lead time from 10 days up to 90+ days, mainly by combining statistical analysis with coupled numerical prediction models. The overall study will be conducted with three Research Objectives (RO). First, the teleconnections between the major global climate driving factors and seasonal and intraseasonal rainfall variation over Northern Ethiopia will be investigated. Next, a numerical model (WRF model) that couples the ocean with the atmosphere will be customized as a regional/local climate model for seasonal and sub-seasonal rainfall prediction over Northern Ethiopia. Following the optimization of the model, as the study will be conducted in an area with a complicated climate system and complex topography, the sensitivity of initial and boundary conditions such forcing initials from different GCM products, ocean-atmospheric variables (from RO1) and terrain complexity in reproducing the JJAS rainfall will be assessed. Finally, a joint atmospheric-terrestrial modelling (WRF-Hydro model) for seasonal and sub-seasonal river flow and soil moisture prediction in the Upper Tekeze river basin will be conducted. At every step of modelling, the performance of the models will be assessed using a series of error statistical methods. The main expected outputs from this research will be the teleconnections of oceanic-atmospheric variables with JJAS rainfall variations; and improved seasonal and sub-seasonal rainfall, river flow and soil moisture prediction models.

Keyword: *Teleconnection, sub-seasonal-to-seasonal prediction, JJAS rainfall Ethiopia, SST, Zonal Wind, Terrain complexity, initial and boundary conditions, WRF model and Coupled WRF-Hydro modelling*

1. Introduction

1.1. Background

Weather is among the critical factors which can strongly influence the socio-economy of a given community (Aggarwal, 2013; Frédéric et al., 2012). Understanding weather and climate characteristics of the past and future is essential for different climate-sensitive sectors such as water resources, agriculture and health. Future weather forecast based on the initials of the atmosphere and boundary conditions of the land surface (White et al., 2017) is widely established with the aim to benefit the end-users/producers. Currently, end-users are demanding reliable forecasts of both direct meteorological parameters and derived information (i.e., extreme events and the degree of their severities) for better preparedness, yield production and management (Klemm and McPherson, 2017). However, due to the chaotic nature of the atmospheric system, reliable and accurate predictions of the future hydro-meteorological components at longer timescales is highly challenging (Schepen et al., 2012). The short-medium weather forecasts (< 10 days) are in a more advanced way that works as an operational forecasting system for mobiles phones, televisions and computers everywhere in the world (WMO, 2018). The long-range (climate) predictions (> 30 days) are also among the widely established methods with relatively fair prediction skills (Frédéric et al., 2012; White et al., 2017) which are employed in different management sectors such as climate hazards (Murphy et al., 2001), agricultural production (Brown et al., 2018; Hoogenboom et al., 2007; Klemm & McPherson, 2017; McIntosh et al., 2007; Zinyengere et al., 2011), health (Harrison et al., 2008) and water resource (Harrison et al., 2008; Nijssen et al., 2001; Wilby et al., 2004; Wood et al., 2004). For instance, Zinyengere et al. (2011) used seasonal climate forecasts in Zimbabwe to improve maize production which helped to achieve remarkable results. Nevertheless, the extended-range predictions that fill the gap between short weather forecast to long-range climate prediction are stated as "predictability desert" (Frédéric et al., 2012; Robertson & Tippett, 2017; White et al., 2017) because of less attention and its difficult timescale to predict. This prediction timescale is worst in areas with complicated climate system and less computing resources like Ethiopia (Nicholson, 2014), and even for weather and seasonal climate predictions.

In Ethiopia, since late 1900s, some studies (Camberlin et al., 2001; Camberlin & Philippon, 2002; Degefu et al., 2017; Diro et al., 2008, 2011a, 2011b; Diro et al., 2012; Funk et al., 2016; Gleixner et al., 2017; Stephanie et al., 2017; Kerandi et al., 2018; Korecha & Barnston, 2007; Korecha & Sorteberg, 2013; Nicholson, 1986, 2014, 2015; Segele & Lamb, 2005; Segele et al., 2009; Segele et al., 2015; Seleshi & Zanke, 2004; Shanko & Camberlin, 1998; Zaroug et al., 2014) were conducted to investigate the predictability of the seasonal rainfall variations. Many of the research outputs (e.g. Degefu et al., 2017; Diro et al., 2008; Gissila et al., 2004; Korecha & Barnston, 2007; Korecha & Sorteberg, 2013) are based on statistical methods. Most of these researches concluded that the main rainy season (locally known as Kiremt which spans from June to September-JJAS) in Ethiopia can be forecasted 2-3 months in advance mainly based on Sea Surface Temperature (SST) anomalies of the El-Nino Southern Oscillation (ENSO), Indian Ocean Dipole (IOD), and Northern Atlantic Ocean (NAO) while including the regional and local atmospheric variables increased the skill of prediction. The SSTs were preferred as key prediction factor because they exhibit a relatively slow change over time and are capable in coupling the ocean and the atmosphere (Diro et al., 2011b; Kumar et al., 2013). For example, Diro et al. (2008) investigated that the Kiremt season in Ethiopian is negatively correlated with Sea Surface Temperature (SST) anomalies of ENSO and IOD, while the JJAS rainfall in the northern part of Ethiopia positively correlated with the Eastern Equatorial Atlantic (Gulf of Guinea). While Korecha and Barston (2007) favoured ENSO only with northern summer. They

emphasized that the ENSO oscillation has a negative impact on Ethiopian rainfall. This implies a dry JJAS rainfall is directly associated with the warmer ENSO.

Moreover, recent studies (Nicholson, 2014, 2015, Segele et al., 2009; Segele et al., 2015; Zeleke et al., 2013) revealed the predictability of the Ethiopian JJAS rainfall is rather strongly associated with the regional and local atmosphere circulations. As per Segele et al. (2009), the Ethiopian Kiremt rainfall variation is more linked with the major Wavelet-Filtered atmospheric components such as zonal winds and pressure highs. Though the degree of atmospheric factors is strongly influenced by the ENSO and Quasi-Biennia Oscillation (QBO) anomalies, their direct link with the regional monsoon system strongly affects the JJAS rainfall of East Africa. In fact, the skill of prediction can be greatly improved when both the regional atmospheric variables and SST anomalies are combined (Nicholson, 2014). For many years, the Ethiopian JJAS rainfall variation was associated with the annual migration of the Intertropical Convergence Zone (ITCZ) from 15^{o}N to 15^{o}S and moving back from the southern hemisphere to the northern hemisphere (Diro et al., 2008; Nicholson, 1986, 2014; Segele & Lamb, 2005). For instance, Northern Ethiopia gets JJAS rain when the ITCZ is starting moving from 15^{0}N in June, while southern Ethiopia is having spring rain during the passage of ITCZ to the southern hemisphere in April (Segele et al., 2009). However, Nicholson (2018) has suggested that it is difficult to link the seasonal rainfall cycle of the Horn of Africa solely with the seasonal migration of the ITCZ.

Considering the aforementioned sources of predictors, coupling the ocean-atmospheric variables for Ethiopian JJAS rainfall be crucial to improve the prediction skills. The ocean-atmospheric variables can be regionalized from the General Circulation Model (GCM) hindcasts through either statistically or dynamically downscaling (Simon, 2008; Tang et al., 2016). Statistically downscaling refers to the use of regional simulation models based on the statistical relationships between the large-scale ocean-atmospheric variables and observed variables. While the dynamically downscaling of GCMs refers to the use of the initial and boundary conditions from GCM products for forcing and verifications of Regional Climate Model (RCM). In the Horn of Africa, particularly in Ethiopia, efforts on seasonal rainfall forecasts based on coupled global climate generating models (Abdelwares et al., 2017; Degefu et al., 2017; Gleixner et al., 2017; Stephanie et al., 2017; Zaroug et al., 2014; Zeleke et al., 2013) have shown great promises. Degefu et al. (2017) demonstrated the ability of the coupled atmosphere-ocean Global Circulation Models (AOGCMs) such as Hadley Centre Global Environmental Model, version 2 (HadGEM2) and Hadley Centre Global Environmental Model, version 3-Global Atmosphere 3.0 (HadGEM3-GA3.0) models to forecast the Ethiopian Kiremt rainfall in relation to seasonal SST anomalies. Gleixner et al. (2017) used ECHAM5 model to investigate the physical link between SST anomalies of ENSO and the Ethiopian Kiremt rainfall, while Zeleke et al. (2013) investigated the teleconnection of the Ethiopian JJAS rain with zonal winds such as low-level winds (850-100hPa) and upper-winds (100-300hPa) using fourth generation RCM (ReCM4) model. These use of ReCM4 have shown good improvement in the forecast skill and have recommended (Zaroug et al., 2014) to be used as a regional model for seasonal rainfall prediction over East African. This has been further confirmed by Gleixner et al. (2017) in that the correlation between simulated rainfall and JJAS rainfall over Northern Ethiopia has been over 53%, while Zeleke et al. (2013) concluded that the use of ReCM4 model exhibits good correspondences, with a correlation around 60%, both spatially and temporally.

The use of dynamically joint ocean-atmospheric climate models such as RCM prediction might be more realistic and greatly improved the skill of the predictions (Simon, 2008). For instance, the Weather

Research and Forecasting (WRF) model (Skamarock et al., 2008) with the European Centre for Medium-Range Weather Forecasts (ECMWF) reanalysis products as initial and boundary conditions were used as regional climate model for East Africa (Abdelwares et al., 2017; Kerandi et al., 2017; Pohl et al., 2011). The result has revealed that the seasonal forecast skill is strongly improved with a 50-80% correlations to the in-situ observations. Numerical weather and climate prediction models involve a great deal of skill to predict the future phenomenon of the climate system compared to statistical prediction methods (Simon, 2008; Warner, 2011). The statistical models require low computing resources compared to dynamic models. The disadvantage of statistical prediction models is, however, the need for long recorded data as they are established based on the relationship of past histories. In East Africa, the sparse distribution meteorological stations and poor quality of observed data are serious drawbacks to use statistical downscaling (Kerandi et al., 2018). Regardless of the demand for high computing resources, dynamically coupled ocean-atmospheric models have superiority over that of statistical prediction methods and the dynamic atmospheric models (Simon, 2008).

In line to this, the issue of good or bad Kiremt season depends on the time of onset and secession, the frequency and duration of wet and dry spells and indeed, the amount of rainfall (Segele & Lamb, 2005). In Ethiopia, a series of extreme events (droughts) have happened in the past (Gebrehiwot et al., 2011; Zeleke et al., 2017). These extreme seasons are correlated with major changes in atmospheric and ocean circulation (Nicholson, 2014; Zeleke et al., 2017). For instance, the drought study by Zeleke et al. (2017) has revealed that the trends of the Ethiopia drought can be predicted in relation to the SSTAs of ENSO. It is expected that reliable and accurate weather and climate prediction can improve the simulation and predictions of hydrological variables (Givati et al., 2012; Verri et al., 2017). To this end, simulating the water balance components for a given basin by coupling the atmosphere with the terrestrial condition has shown great improvements (Givati et al., 2012; Kerandi et al., 2018; Srivastava et al., 2015). Especially, in arid and semiarid areas where the level of soil moisture is strongly governed by rainfall variations (Kerandi et al., 2018), joint atmospheric-hydrological modelling significantly improves the quality of model simulations.

Therefore, the aim of the study is to develop/customize site-specific numerical models that enable seasonal and sub-seasonal rainfall and river flow prediction with a lead time of 10 days to four months for the Upper Tekeze River Basin, Northern Ethiopia. In World Meteorological Organization (WMO) bulletin 61 (Frédéric et al., 2012), understanding the mechanisms and the model physics, evaluating the skills and estimating uncertainties of sub-seasonal to seasonal (s2s) predictability of the weather and climate have been mentioned as key research priorities. This is because decision making in many sectors such as agriculture, water management, insurance, and industry is depending on this timescale. This research is part of the EENSAT project (EENSAT, 2018) and in line with the Ethiopian Agricultural Transformation Plan in that, the issue of weather as a critical factor for sustainable agriculture production and water resources management is addressed.

1.2. Research problem and Justification

In Ethiopia, a strategy on reducing land degradation and transforming agricultural productivity through improved water management have had implemented since the 1990s (ENPC, 2016; Lakew et al., 2005). As a result, various water infrastructures (Berhanu et al., 2014) such as water harvesting technologies, hydropower, and small-scale irrigation schemes had been established. These implemented water harvesting technologies were planned to have a profound influence on hydrological response and, in

general, on the socio-economy of the country. However, occurrences of frequent droughts coupled with the unpredictable climate variables especially rainfall and runoff were indicated to be the major threats for sustainable development and management (Gebrehiwot et al., 2011).

The weather system in Ethiopia is very complex because of the seasonal and interannual variability influenced by numerous atmospheric and oceanic factors and highly complex topography (Diro et al., 2012; Girma et al., 2016; Nicholson, 2014). Due to this fact, the rainy seasons of the country widely vary from place to place (Girma et al., 2016) but are generally categorized as (1) Kiremt: June- September; (2) Belg: February - May and (3) Bega: October -January (NMA, 2018). Understanding the characteristics of the main rainy season (JJAS rainfall) and reliable predictions are essential because (1) predicting the JJAS season rainfall means covering 60% of Ethiopia's main rainfall season-Kiremt (Segele & Lamb, 2005). This also extends to the Sahelian countries to the west and east to the Horn of Africa (Nicholson, 2014, 2015; Segele et al., 2009); 60-85% of the annual average rainfall (Figure 4.2) is collected from the Kiremt season (Segele & Lamb, 2005); (2) more than 85% of the Ethiopian population depends on rain-fed agriculture (Degefu et al., 2017; Diro et al., 2011a; Gleixner et al., 2017) mainly from this season; and (3) 85-90% of the annual crop yield are harvested from this season (Gissila et al., 2004).

The Ethiopian seasonal rainfall distribution has been classified into different homogenous regions (Figure 2.2). For instance, the Ethiopian rainfall seasonality has been classified into 14 regions (Zeleke et al., 2013); eight regions (Girma et al., 2016); eight regions but with different geographical locations (Korecha & Barnston, 2007); five regions (Diro et al., 2008, 2011a, 2011b); five regions but with different geographical location (Gissila et al., 2004): four regions (NMA, 2018): three regions (Degefu et al., 2017); and two regions (Nicholson, 2014, 2015). None of the studies has agreed to a common regionalization (Figure 2.2). For example, the Northern Ethiopia rainfall (Figure 2.2 green box) is regionalized under Cluster I (Gissila et al., 2004) which covers only the northern part of the country, whereas Diro et al. (2008) divided the region into two zones: Zone-I and Zone-IV. In Diro et al. (2008), the Zone-I covers the northwest part of Ethiopia, while the Zone IV covers half of Tigray, Afar, and eastern Amhara regions up to northern part of Oromia. Moreover, the National Meteorological Agency (NMA) forecasting system (NMA, 2018) for Northern Ethiopia rainfall (particularly for Upper Tekeze river basin) uses a completely different cluster than the above studies (Figure 2.2F).

The demand for skilful hydro-meteorological forecasts is highly increasing for site-specific decision-making in several sectors. In Ethiopia, in general, there is low skill regarding seasonal rainfall and river flow predictions. For seasonal (long-range) rainfall predictions, the NMA uses the analogue year method (NMA, 2018) based on trend analysis and statistical assessment of SST of ENSO (Korecha & Sorteberg, 2013). This could be since the model requires less computational resources and simplicity. The skill for the seasonal prediction is categorized from weak to moderate with a Ranked Probability Skill Score (RPSS) of 10% and is biased towards nearly-normal rain (Korecha & Sorteberg, 2013). This indicates that the forecasting system fails to properly capture the rainfall events below (drought) and above (flooding) normal categories. For example (Figure 1.1), during the drought year of 2009 over Northern Ethiopia, the Ethiopia NMA forecasts around 25% of its tercile probability as below normal precipitation, while the observed shows the precipitation below normal condition was more than 80%.

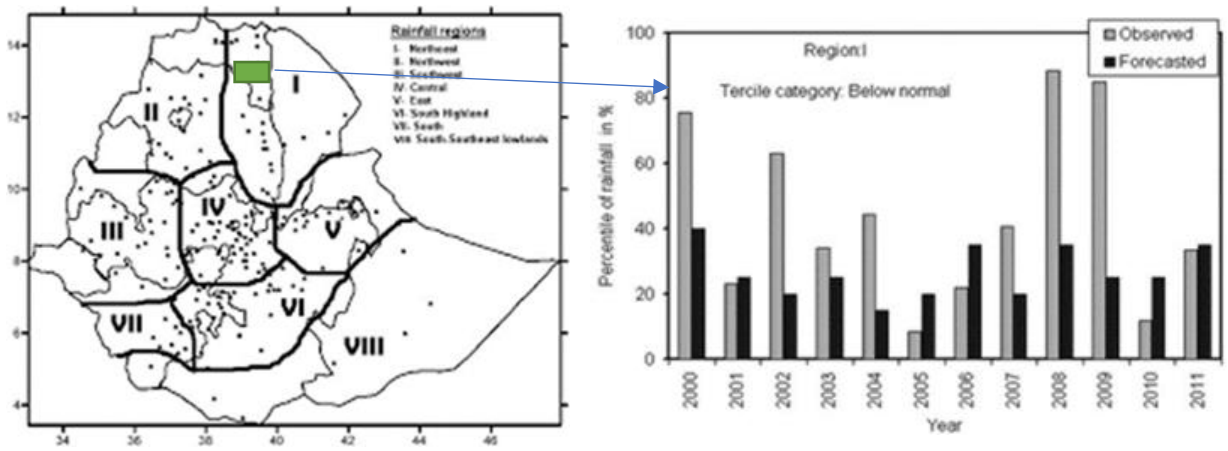

Figure 1.1. comparison between the total observed and predicted Kiremt season rainfall (on the right) for region I (green box on the left), Northern Ethiopia. Adapted from Korecha and Sorteberg (2013)

This might be due to the fact that, for the Ethiopian climate system, a prediction for all these different regions with a single method becomes unreliable and therefore has a low predictive skill (Degefu et al., 2017; Gissila et al., 2004). In addition, seasonal predictions over any region are incomplete without proper treatment of the land surface, oceanic and atmospheric parameters (Camberlin et al., 2001; Diro et al., 2008). In order to improve the forecast, detailed studies with better methods such as using hybrid models (Schepen et al., 2012) that considers most underlying factors of the ocean and atmospheric variables need to be considered (Camberlin et al., 2001; Diro et al. 2008; Zeleke et al. 2017). The use of the hybrid model (section 2.3) for seasonal and sub-seasonal rainfall prediction over Northern Ethiopia is limited. This calls for a comprehensive study on all the teleconnections (potential predictors), i.e., which indicator and how strongly these are associated with Ethiopian Kiremt rainfall is essential. It has been reported (Huang & Gao, 2017; Jee & Kim, 2017; Noble et al., 2017; Quitián-Hernández et al., 2018) that , in areas with complex climate system, combining use of the statistical models (i.e., selecting appropriate predicator in relation to predictands) with dynamical models can significantly improve the skill of predictions. This was supported by Korecha & Sorteberg (2013) in that the NMA prediction skill can be improved if all the climate driving factors associated to the Ethiopian rainfall are considered using numerical models.

For JJAS rainfall predictions, some studies in East of Africa, for example (Degefu et al., 2017; Diro et al., 2008, 2011b, 2011a; Nicholson, 1986, 2014, 2015; Zeleke et al., 2013), have developed statistical methods based on teleconnections. These studies concluded that the JJAS rainfall prediction can be possible in relation to three teleconnections: (1) remotely SST anomalies, (2) regional and local atmospheric variables and (3) combining the SST with the atmospheric variables. Majority of the studies (e.g. Korecha & Barnston, 2007; Degefu et al., 2017; Diro et al., 2008, 2011a, 2011b) have agreed that the JJAS rainfall predictability can be mainly based on remotely SST anomalies of ENSO and IOD, and while the others (such as Segele et al., 2009; Zeleke et al., 2013) have argued that the JJAS rainfall variations are strongly correlated with regional and local atmospheric variables such as Tropical Eastern Jet (TEJ) and other zonal wind pressures than that of SST anomalies. These prediction methods have shown good correspondence, up to 60-80% correlations but with high temporal and spatial inconsistency. These inconsistencies could be due to the fact that the statistical methods were developed based on the relationship between the predictors and predictands from different regions, with less than 50% correlations between observed variables within the clusters (Diro et al., 2008). The general conclusions from these studies are that the

skill of forecasts was improved when SST anomalies combined with that of the regional and local atmospheric variables are used. This has been, for example, confirmed by Nicholson (2014) in that the JAS rainfall over the Horn of Africa is strongly linked with SST anomalies of ENSO (-0.71 correlation) and sea level pressure in the central equatorial Indian ocean (-0.57) and atmospheric circulations such as zonal winds (200mb) in the western equatorial Indian ocean (-0.61). Though the ENSO contributes 49% of the variations, the overall predictability was enhanced while the SSTs combined with the atmospheric variables, with a correlation up to 81%. Hence, coupling the ocean-atmospheric variables using either numerical (Warner, 2011) or a hybrid model (Schepen et al., 2012) can be required to incorporate all the possible predictors for JJAS rainfall in Northern Ethiopia.

For the last 50 years, Ethiopia suffered from severe and recurrent droughts, and most of these recurrent droughts occurred during the main rainy season (Segele and Lamb, 2005). These extremes have had a significant impact on agriculture, hydrological states and thus the food security in Ethiopia. For instance, in Northern Ethiopia, the drought of 2009 (Korecha & Sorteberg, 2013), 2010/11 (Nicholson, 2014) and 2015 (Funk et al., 2016) have created a substantial crisis in the country. However, the effort to investigate the severity, magnitude and when it will happen again is insufficient. Although there is little, we can do to prevent droughts and/or flooding, we can improve our preparedness for these events which in turn relies on the availability of sound information. While there are more advanced prediction models at high resolutions such as numerical weather and climate models (Simon, 2008; Stensrud, 2007; Warner, 2011), except for the short-range weather forecasting, however, the NMA operational forecasting is still suffering from unreliable and inaccurate forecasts. For example, the recent seasonal rainfall and river flow forecasts for JJAS 2018, was not very well captured by NMA. There was excess rain and consequently flooding. As a safety measure, a lot of water was discharged from the Tekeze dam to prevent overtopping (TigrayTV, 2018a). The local media (TigrayTV, 2018b) has broadcasted that more than 180 ha of irrigated lands were damaged due to the excess water released from the dam in a plan to rescue the dam. To address these issues, a comprehensive investigation of the Ethiopian Kiremt season variability, its teleconnections, and the skill to predict a few months in advance for efficient operating water infrastructures and effective mitigating disasters are essential.

At this moment, the gap between subseasonal-to-seasonal prediction is not investigated and neither used by NMA during operational forecasting. There is also limited progress on dynamical prediction for the greater Horn of Africa region, particularly for Ethiopia despite the availability of high technologies elsewhere in the globe. Moreover, research results regarding the ocean-atmosphere-land surface interaction in Northern Ethiopia from a few weeks to a few months in advance are not available.

1.3. Significance of the study

The Ethiopian development strategies have a high demand for reliable and accurate hydro-meteorological time series (i.e., past-present-future) data for proper designing, implementing and sustainable monitoring of agricultural and water infrastructure schemes. However, the field of hydro-meteorology is among the data scarce sectors of the country. The number of meteorological stations is insufficient (sparsely distributed network) with many gaps and it is also hard to find long-term streamflow data even for the major rivers. These gaps can be filled by generating synthetic data through research and technology adaptations from the best experiences of the international community. Nowadays, there are various community based open resources, such as WRF and WRF-hydro models, that can be utilized in a wide range of applications (Powers et al., 2017) and customized depending on the regional and local climate

characteristics (Abdelwares et al., 2017; Pohl et al., 2011). To this end, this research will work in line with the demand which is listed as follows:

- The seasonal and subseasonal rainfall forecasts/anomalies over Northern Ethiopia can be improved, simulated and forecasted, based on the teleconnection with the ocean-atmospheric anomalies.
- Seasonal and sub-seasonal rainfall forecast for Northern Ethiopia in few weeks to few months in advance can be further improved using hybrid models by combining the statistically correlated teleconnection of the ocean-atmospheric variables with numerical prediction models. For this, there are several research and experiences elsewhere (internationally and few attempts locally).
- Streamflow for major rivers can be reliably and accurately simulated with few weeks to four months in advance by understanding the seasonal and sub-seasonal weather variations coupling with the terrestrial characteristics such as land use/land cover dynamics.
- Extreme events such as seasonal droughts (both agricultural and hydrological) are among the major threats to the Northern Ethiopia that can be attributed to extreme weather variations leading to severe drought. Understanding and providing information regarding the spatiotemporal characteristics mainly in relation to extreme weather events with a lead time of 10 days to four months is possible. For this, there are available tools and technologies

2. State-of-the-art seasonal and sub-seasonal prediction

Reliable and accurate hydro-meteorological prediction in lead time of a few months ahead is being at the centre of interest for many researchers (e.g. Aggarwal, 2013; Parker et al., 2008; Siddique et al., 2015; Vitart et al., 2014). Accurate prediction requires a good understanding of the physical laws of the ocean-atmospheric-land surface interactions and well representations of the weather phenomenon (White et al., 2017). However, the issue of reliable and accurate hydro-meteorological forecasts at seasonal and sub-seasonal timescales is highly challenging and "a distant dream" for scholars (Aggarwal, 2013; Schepen et al., 2012). This is due to the fact that climate variables are the result of the chaotic nature of the atmosphere-land surface-ocean system interactions (Kirtman et al., 2014). Recently, there are various success stories of weather and climate predictions with different lead time (e.g., Guo et al., 2014; Murphy et al., 2001; Schepen et al., 2012; Segele et al., 2015). Based on the predictability skill and sources of predictors (Figure 2.1), these weather and climate forecasts can be categorized (Tian et al., 2018; White et al., 2017) as (1) weather forecasting (one-10 days), (2) sub-seasonal (weather-to-climate) prediction (10 –30 days) and (3) seasonal climate prediction (30-90+days). White et al. (2017) illustrated that the predictability of short-medium range forecasting is mainly due to initial conditions from the atmospheric circulations, while for seasonal predictions, the initial condition of the ocean-land surface interactions such as remotely SSTAs of ENSO is found crucial. The sub-seasonal prediction fills the gap in between these two ranges of forecasts. The predictability of sub-seasonal-to-seasonal (s2s) depended on the initial conditions of the atmosphere such as Madden-Julian Oscillation (MJO) and QBO, and the boundary conditions of the ocean-land surface interactions such as soil moisture and SSTs of ENSO, IOD and Atlantic Ocean Dipole (NASEM, 2016; White et al., 2017).

Weather and seasonal climate prediction are well investigated (Frédéric et al., 2012). However, the weekly averages which extended from medium-range weather prediction to long-range climate prediction are not being well explored (White et al., 2017). This shows that prediction the ocean-atmospheric-land

surface interaction with the timescales of a few weeks in advance is very difficult. Nevertheless, there is great progress to bridge the gap between the weather and climate prediction i.e., at s2s scale (Frédéric et al., 2012, 2018; Olaniyan et al., 2018; Tian et al., 2017). Compared to seasonal climate forecasts, predictions of weather-to-climate variables have large societal benefits for many management decisions such as water resources and agriculture (Frédéric et al., 2012; Tian et al., 2017; Vitart et al., 2014; White et al., 2017). For example, the agriculture sector is strongly depending on two weeks to 3 months' time intervals of the rainfall amounts, intensity, onset and recession, and its extreme (Vitart and Robertson, 2018).

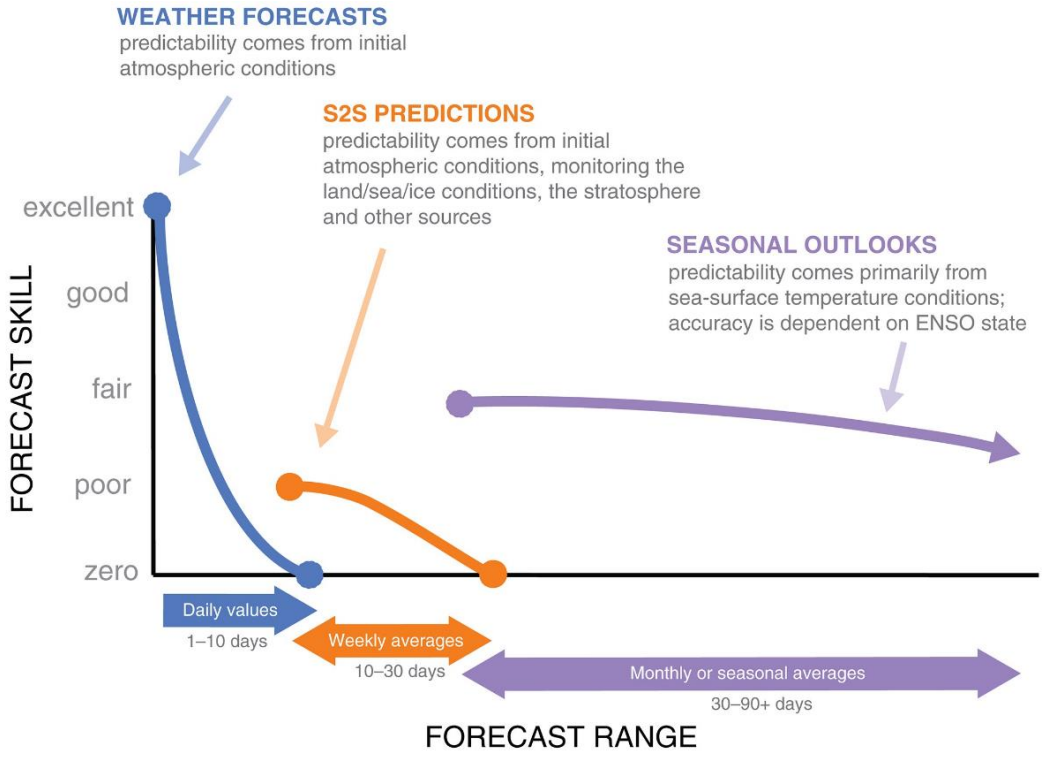

Figure 2.1: Climatological prediction ranges from short-range weather forecasts to long-range seasonal climate predictions and potential sources of predictability (White et al. 2017)

Generally, weather and climate predictions at seasonal and sub-seasonal timescales can be excuted using three approaches (Aggarwal, 2013; Diro et al., 2012; Wang et al., 2012): (1) statistical, (2) numerical (dynamic), and (3) Hybrid (combing the statistical and dynamic model).

2.1. Statistically seasonal and sub-seasonal prediction

Statistical methods are models that predict the future behaviour of the climate system based on a past relationship with the atmosphere-ocean parameters (Aggarwal, 2013; Diro et al., 2011a; García-Díez et al., 2013). Seasonal prediction using statistical methods is among the widely utilized method of prediction (Djibo et al., 2015; Funk et al., 2014; Guo et al., 2014; Sittichok et al., 2016; Villarini & Serinaldi, 2012). For instance, for East Africa seasonal and interannual rainfall prediction, several statistical rainfall prediction studies (Camberlin et al., 2001; Camberlin and Philippon, 2002; Indeje et al., 2000; Kerandi et al., 2017; Nicholson, 1986, 2014, 2015), and particularly for Ethiopia (Camberlin,1997; Degefu et al., 2017; Diro et al., 2008, 2011a, 2011b; Elsanabary & Gan, 2012; Gissila et al., 2004; Korecha and Barnston, 2007;

Korecha and Sorteberg, 2013; Parker et al., 2008; Segele and Lamb, 2005; Segele et al., 2009, 2015; Seleshi and Zanke, 2004; Shanko and Camberlin, 1998) have been conducted. These studies are based on the statistical relationship of oceanic variable and rainfall and/or oceanic-atmospheric variables and rainfall. These statistical relationships are developed using four approaches: (1) analogue method (the one that the NMA uses), (2) weather generator models (GCMs and RCMs), (3) regression models and (4) discriminant analysis methods. Of these, the regression models and statically downscaling methods are among the widely applied methods because of their small demand for computing resources and its relatively easy to understand (Tang et al. 2016).

The result from these studies have revealed that the JJAS rainfall over East Africa, particularly over Ethiopian, is strongly associated either with remotely oceanic anomalies such as SSTs of ENSO, IOD and AOD and/or the regional and local atmospheric circulations such as the position of ITCZ, zonal winds like Tropical Easterly Jet (TEJ) and pressure highs such as Mascarenes and St. Helena. More specifically, they have found that the JJAS rain predictability greater than 2-3 months in advance is difficult. For instance, Diro et al. (2008, 2011a) have performed detailed investigations on the teleconnections between the Ethiopian rainfall and the oceanic region and the lag-time of the predictors across different regions. They used stepwise regression with two sets of predictors and 8 months lag-time. Their findings exhibited that, for example, the JJAS rainfall in Northern Ethiopia is positively associated with the northwest Pacific Ocean and the Gulf of Guinea, with a lag time of 1-2 months. More noticeably, almost all the studies have agreed that the prediction skill of these statistical methods is inconsistent both specially and temporally. This can be because of the complicated climate system and complex topography over east Africa (Diro et al., 2011a; Korecha & Barnston, 2007; Nicholson, 2014; Zeleke et al., 2013). To consider the spatial complications into account, all statistical studies for rainfall prediction have used regionalization, with no one region in common (Diro et al., 2008, 2011a; Gissila et al., 2004; Korecha and Sorteberg, 2013). It is expected that from different regionalization and different use of teleconnections, their findings (for example, for the same locations like at watershed level) is found different. For example, the JJAS rainfall in Northern Ethiopia (a green box in Figure 2.2) has: a weak but negative correlations with global SST anomalies of the of IOD and ENSO (Figure 2.2a: Gissila et al., 2004), a strong and positive relationship with northwest Pacific Ocean and Gulf of Guinea SST anomalies (Figure 2.2b: Diro et al., 2008); a negative correlation with ENSO (Niño-3.4) SST anomalies (Figure 2.2c: Korecha and Sorteberg , 2013) ; and a negative correlation with ENSO and IOD SST anomalies (Figure 2.2e: Degefu et al., 2017).

Statistical model outputs are less preferable by end users (Klemm & McPherson, 2017). They are expressed in two ways of probability displays: tercile/quartile maps and (2) the probability of exceedance (PoE) graphs (Klemm and McPherson, 2017). The tercile is a commonly used form of statistical prediction (Klemm and McPherson, 2017). Klemm and McPherson (2017) indicated that though the PoE graphs are less common, they are preferable than that of the tercile maps. The tercile maps have been criticized by end users for the facts that (1) they do not clearly show the spatial details; (2) the maps are not in user-friendly format for communications, (3) they lack enough skill to be used for decision making, (4) they do not have information on forecast uncertainty, and (5) they do not quantify how to deviate the forecast of below normal or above normal precipitation from that of the normal precipitation. This can be clearly observed in the NMA forecast for 2018 Ethiopian Kiremt rainfall (Figure 2.2f). For instance, the region in zone two from the top (Figure 2.2f) includes the wettest region from the West through the moderately wet in the middle to the driest part of the East Ethiopia with equal tercile probability of 40% above normal, 35% nearly normal and 25 % below normal. How representative are these probabilities in

such widely different geographical settings? These forecasts did not even clearly show how spatially varies, while, regions with relatively dry zones such as the Afar region have suffered from the low amount of rainfall.

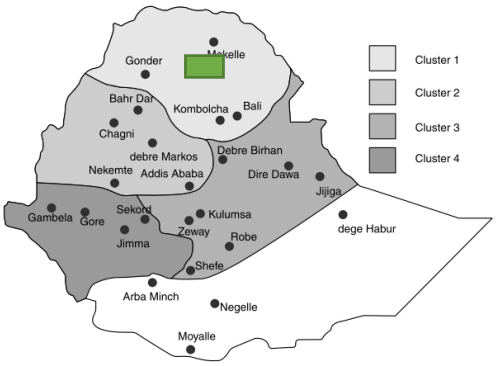

a(Gissila et al., 2004)

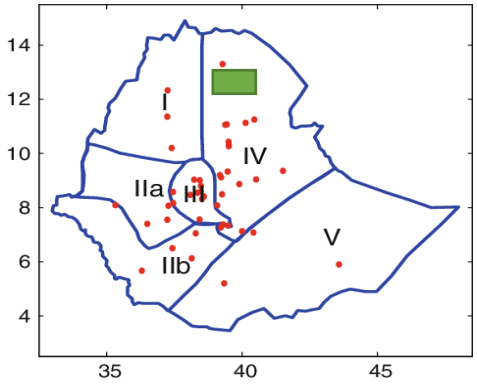

b(Diro et al., 2008)

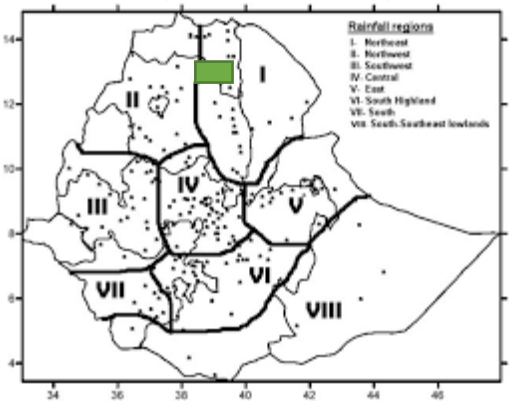

c (Korecha & Sorteberg, 2013)

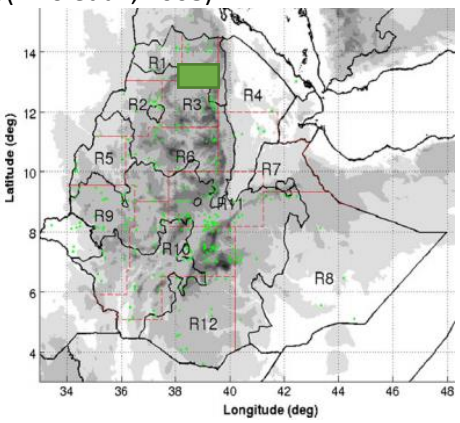

d(Zeleke et al., 2013)

e(Degefu et al., 2017)

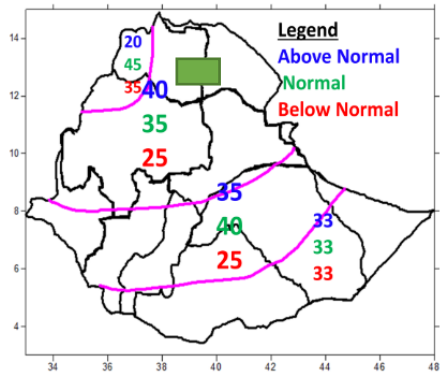

f(NMA, 2018)

Figure 2.2 Regionalization of Ethiopian rainy season from different sources including ENMA (a-f). The green box represents an arbitrary location of the study area.

2.2. Numerical Weather and Climate Predictions (NWCP)

Numerical weather prediction (dynamic modelling) refers to the forecasts based on the physics of atmospheric-oceanic interactions (Simon, 2008; Stensrud, 2007; Warner, 2011). This can be carried out by calibrating and validating raw outputs from global prediction models. Based on their initial and

boundary condition requirements, NWCP models are classified into two (Simon, 2008; Warner, 2011): (1) uncoupled climate models and (2) fully-coupled climate models. In an uncoupled climate model, atmospheric variables are the only parameters considered in the dynamic model while the lower boundaries are specified manually (Simon, 2008; Stensrud, 2007; Warner, 2011). Whereas in fully-coupled models, all the relevant components of the atmosphere and boundary conditions are modelled and predicted simultaneously (Aggarwal, 2013; Simon, 2008). Uncoupled models need less computational costs compared to that of the coupled model. Nevertheless, the fully-coupled climate model provides the most realistic information on the climate system (Simon, 2008). The basic assumption in uncoupled climate models is that the effect of ocean parameters such as SSTs to atmospheric circulation is only one way. This assumption strongly deviates from the fact that the land surface variables influence the atmospheric climate and in turn, the atmospheric variability affects the ocean conditions (Kumar et al., 2013; Simon 2008). Therefore, the fully-coupled model is more capable of producing better and reliable forecasts than uncoupled counterparts.

For complex climate systems where the skill of prediction improves when the remotely SST anomalies are combined with the regional and local atmospheric circulation, fully-coupling dynamic models are very essential (Simon, 2008). Globally, forecasts based on fully coupled ocean-atmospheric circulation have shown significant skill improvements. For instance, the ECMWF at 1° horizontal, and L91 and L75 vertical resolutions for ocean and atmosphere, respectively (Stockdale et al., 2018), GFS at 0.25^{o} horizontal and L64 vertical resolutions (GFS, 2018), CFSV2 at 0.2-2.5^{o} horizontal and L64 (0.3hPa) vertical resolution (Saha et al., 2014), ECHAM6 at L47/L95 (800hpa) horizontal resolution (Stevens et al., 2013), GloSea5 at horizontal resolution in the atmosphere (N216–0.7◦) and the ocean (0.25◦), and L85 vertical resolution (MacLachlan et al., 2015) and GEOS-5 at 1° × 1.25° horizontal and L72 vertical resolution (Borovikov et al., 2017) are among the widely applied large-scale weather and climate prediction models. Theses GCM models forecast basic climate components for a wide range of temporal scales, for example, from days to several months in advance. Moreover, the ECMWF (Vitart et al., 2014), and CSFv2 (Saha et al., 2014) models have the potentials to predict climate variables at sub-seasonal timescale, up to 32 days and/or 3-4 weeks in advance. Olaniyan et al. (2018) evaluated the capacity of the ECMWF model to simulate the s2s atmospheric circulations that affect the monsoon in West Africa. They conclude that the ECMWF model is capable and reliable to predict the major atmospheric and oceans variables in West Africa. Saha et al. (2014) evaluated the forecasts from the CFSv2 model in that they concluded that the model has good skill for seasonal and sub-seasonal rainfall forecast in the United States and SST forecasts globally.

The most difficult task in regional and local weather and climate prediction system at seasonal and sub-seasonal timescale is to consider all climate components that could play a great role in predictions (Simon, 2008; Stensrud, 2007). Dynamical downscaling of the initial and boundary conditions from GCM models to a finer resolution such as to regional and local climate may provide necessary information (Diro et al., 2012). The downscaling provides improved local ocean-atmosphere information by nesting the coarser boundary condition with the smaller domains (Diro et al., 2012; Tian et al., 2017). This can be carried out either statistically or dynamically. For instance, in Ethiopia where the study area is found, the GCM products such as from ECMWF, ECHAM and GFS have downscaled into regional scales using different statistical and numerical models. Stephanie et al. (2017) compared the capability of 11 GCMs including the ECMWF, ECHAM, and GFS to predict the Ethiopian Kiremt rainfall using statistical downscaling models. They have found that the ECMWF seasonal hindcasts have shown better skill to predict JJAS rainfall, with a correlation of 0.53. Tian et al. (2017) downscaled the CFSv2 daily forecasts for sub-

seasonal precipitation prediction for which the regional model enabled to reproduce weather forecast up to 30 days in advance. Regardless of computing costs, dynamically downscaling of the ocean-atmospheric variables from GCM products using different regional models are among the reliable and relatively accurate forecasts (Simon, 2008). For example, dynamically downscaling of GCM products using: WRF model for East and West Africa seasonal precipitation and runoff simulation (Kerandi et al., 2018; Kerandi et al., 2017; Ratna et al., 2014; Siegmund et al., 2015), for regional climate simulation in Canary Islands (Pérez et al., 2014), for streamflow prediction in Jordan river (Givati et al., 2012), and for meteo-hydrological modelling in Italy (Verri et al., 2017); using the third generation Regional Climate Model (ReCM3) for Horn of Africa seasonal rainfall prediction (Diro et al., 2012); using National Centres for Environmental Prediction (NCEP) Regional Spectral Model (NCEP-RSM) for operational season climate prediction in Northern Brazil (Hong et al., 1999; Tang et al., 2016); using the MM5, COAMPS and WRF models for seasonal climate prediction in Northern America (Lu et al., 2011) have effectively demonstrated.

Among other RCMs, the WRF model becomes the world's widely acceptable and applicable mesoscale numerical model (Powers et al., 2017). The WRF model is the "next-generation mesoscale NWP system" which offers quite a range of applications and capacities (Powers et al., 2017; Warner, 2011). It is a community-based system developed for both atmospheric research and operational forecasting. The WRF model was publicly released since 2000 and has been maturely grown to afford a variety of earth system predictions such as climate and hydrology at regional and local spatial scales with wider temporal scales (Skamarock et al., 2008). In general, regardless its demand for high computing resources and quite several parameters, the model is more capable to address weather and climate variables at smaller atmospheric scales, dynamically coupling the ocean-atmosphere-land surfaces and link research to operational developments (Powers et al., 2017). Moreover, the WRF model emerges high-level numerical accuracy and scalar conservation properties compared to other RCM such as MM5 (Powers et al., 2017).

2.3. Hybrid (combination of statistical and dynamical) predictions

The Hybrid model denotes the combination of statistical and dynamical methods (Diro et al., 2011b; Schepen et al., 2012). This type of models usually used weather indicators/predictors statistically in good correlations with the observed rainfall (e.g. SSTs) and then used as input into a dynamical atmosphere model such as GCMs for seasonal and subseasonal rainfall forecasts. Though the model is not widely used, some studies (e.g., Schepen et al., 2012; Segele et al., 2009; Vecchi et al., 2011; Wang et al., 2012) revealed that skills of prediction are greatly improved when the statistical methods are combined with that of dynamic models. Schepen et al. (2012), for example, combined statistical and dynamic forecast using Bayesian Model Averaging (BMA) for Australia seasonal rainfall forecast. The researchers demonstrated that the hybrid models have significantly improved the skill of prediction and are capable to capture the maximum spatial and temporal coverages of the rainfall forecast.

2.4. Uncertainties in seasonal and subseasonal predictions

Every seasonal and subseasonal prediction model suffers from biases i.e., the model forecasts deviate to some degree from that of the observed variables (Palmer et al., 2005; Simon, 2008; Stensrud, 2007; Warner, 2011). The accuracy and reliability of forecasts from such dynamic systems are governed by three sources (Figure 2.3): (1) the uncertainties due to imperfect initial conditions (2) the uncertainties due to the model development and (3) limited understanding of the chaotic system (Aggarwal, 2013; Diro et al., 2012; Kirtman et al., 2014; NASEM, 2016; Slingo & Palmer, 2011). In addition, the sparse distribution of observing stations in some parts of the globe may greatly influence the accuracy of the initial and

boundary conditions from GCMs (MacLachlan et al., 2015). Nevertheless, since the 2000s, the seasonal and subseasonal prediction system shows great improvement in two approaches: (1) quantifying the uncertainty of forecasts, and (2) improving the forecast skill using multimodel ensembles (Kirtman et al., 2014; Klemm & McPherson, 2017). To deal with, many studies have been conducted (e.g. Booji et al., 2018; Kusunose and Mahmood, 2016; Palmer et al., 2005; Slingo and Palmer, 2011; Wilks and Vannitsem, 2018). The errors related to initial and boundary conditions can be considered using ensemble forecasts, whereas, the errors arise due to limited understanding of the subject are minimized using the multimodel ensembling (MME) approach (Aggarwal, 2013; Kirtman et al, 2014; Simon, 2008). The aim of MME for seasonal and sub-seasonal predictions is to customize methods that can manipulate the dataset from the multiple outputs of several global coupled ocean-atmospheric models.

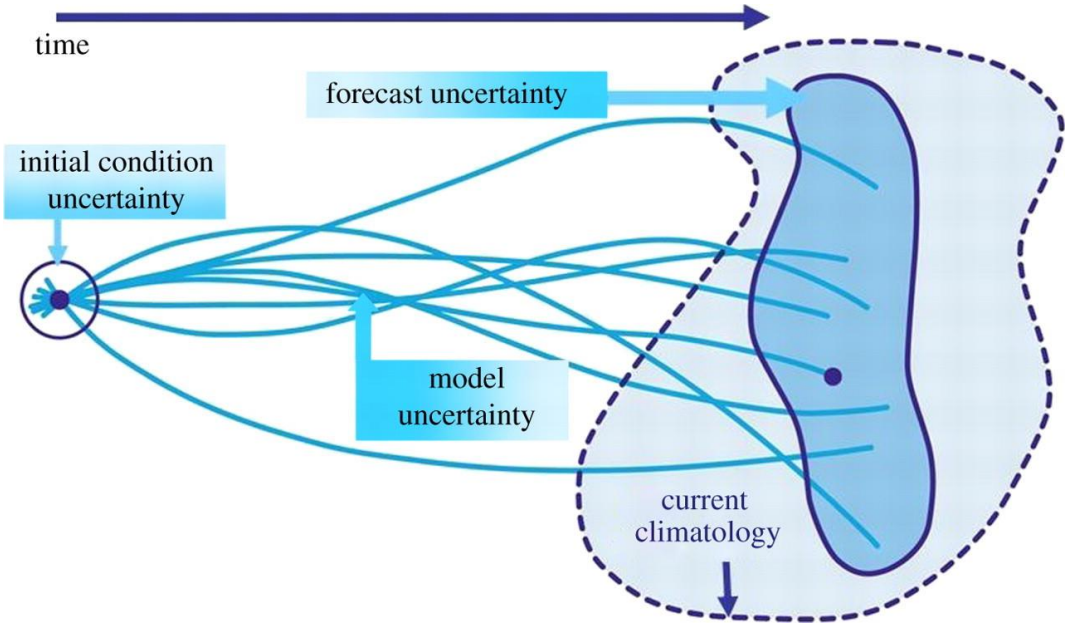

Figure 2.3: Schematic representation of the probabilistic uncertainties in weather and climate prediction due to the initial condition, and the prediction model (Slingo & Palmer, 2011).

As per Aggarwal (2013), the idea of MME is that the ensemble forecast of individual models is taken first to minimize the errors due to imperfect initializations. The ensemble of the ensemble forecasts from single models is therefore followed to consider the errors due to limited understanding of the dynamic system. Kirtman et al. (2014) have demonstrated the performance of MME forecasts and they have found superior skill over the forecasts from single-model. This might be because the errors from individual models can be averaged out when they ensemble. This approach is being used by many researchers, e.g. (Brown et al., 2010; Diro et al., 2012; Gobena & Gan, 2010), to make probabilistic seasonal forecasts of the dynamic terrestrial-atmosphere-ocean interactions. Moreover, the accuracy and reliability of model forests increase if the MME further combined with data assimilation methods (Bourgin et al., 2014; Force et al., 2009). For instance, to consider the uncertainties from the initial condition into account, the WRF model uses 3d var and 4d var data assimilation techniques (Skamarock et al., 2008) and the GloSea5 model uses 3DVar assimilation system and lagged start ensemble techniques (MacLachlan et al., 2015). Besides, the uncertainties raised from incorrect observations and representations can also be minimized by employing proper verification techniques before they are used as prediction tools (NASEM, 2016; Tang et al., 2016).

3. Conceptual framework and research objectives

3.1. Conceptual framework

Based on the aforementioned research gaps, technologies and approaches, this study attempts to investigate the dynamic behaviour of the hydro-meteorology over Northern Ethiopia; and their link to the ocean-atmosphere-land surface interactions. The conceptual framework of the study is presented in Figure 3.1. The major aim of this research work is to improve the hydro-meteorological forecasts (precipitation, runoff and soil moisture) over Northern Ethiopia for the period of 2009-2020/21 at two time-scales: (1) sub-seasonal timescale (10-60 days) and (2) seasonal timescale (four months-JJAS). To conduct this study, first, understanding the ocean-atmospheric phenomenon and identifying the major ocean-atmospheric factors that are strongly correlated with the seasonal and sub-seasonal rainfall variation over Northern Ethiopia is essential. This can be achieved by investigating the concept and theory of the micro and mesoscale physics in detail (White et al., 2017). Secondly, a coupled NWCP model, i.e., the WRF model, will be customized as regional weather and climate model based on the ocean-atmospheric teleconnections associated with the seasonal and sub-seasonal rainfall over Northern Ethiopia. Herein, customization of the WRF model using different rainfall prediction experiments (sensitivity analysis) in relation to WRF model parametrization, initial and boundary conditions (ocean and atmospheric interactions-results from the first step) will be covered. This could help to reliably and accurately predict the weather/climate variables. Finally, the response of the hydrometeorological variables to the ocean-atmospheric–terrestrial interaction will be evaluated using the WRF model extension i.e., WRF-Hydro. The result/output from this work will be analysed using different statistical methods and will have paramount importance for proper management, monitoring and decision making in different sectors such as agriculture and water resources of Northern Ethiopia in particular, and Horn of Africa in general.

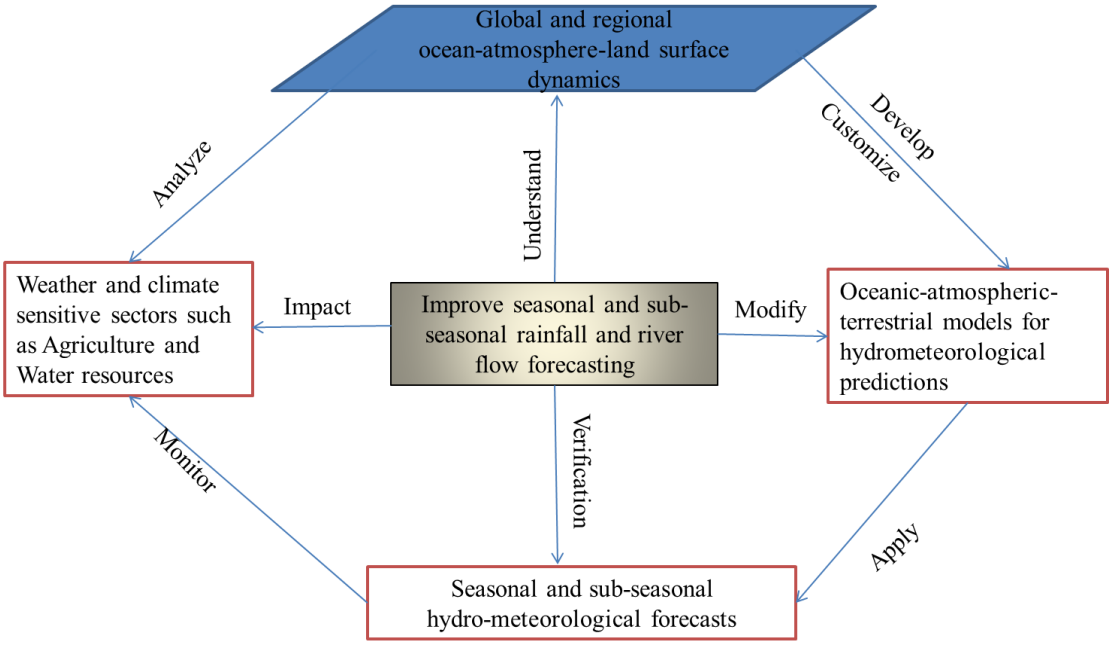

Figure 3.1: The conceptual framework to improve seasonal and subseasonal rainfall and river flow prediction.

3.2. Objectives

The main objective of this research work is to improve seasonal and sub-seasonal hydrometeorological (rainfall, river flow and soil moisture) predictions with a lead time of 10 days to four months (JJAS rainfall) over Northern Ethiopia.

3.2.1 Research objectives (RO)

This study will be carried out with three research objectives:

RO1: Investigate the teleconnections between the major global climate driving factors and seasonal and sub-seasonal rainfall variation over Northern Ethiopia

- Identify ocean-atmospheric variables that link to sub-seasonal and seasonal rainfall in Northern Ethiopia
- Analyse the correlation between the oceanic-atmospheric factors and the JJAS rainfall
- Develop a framework for possible predictions based on the ocean-atmospheric teleconnections

RO2: Customize the WRF model as a regional climate model for seasonal and sub-seasonal rainfall prediction in Northern Ethiopia

- Optimize the physical parameters of the WRF model for seasonal and sub-seasonal rainfall prediction
- Perform a sensitivity analysis of SST, zonal wind, terrestrial complexity and forcing initials from different GCM products in improving the JJAS rainfalls prediction
- Evaluate the performance of model forecasts

RO3: couple the atmospheric to the terrestrial models (WRF-Hydro) for seasonal and sub-seasonal hydrological predictions of the Upper Tekeze Basin in Northern Ethiopia

- Predict the hydrometeorological variables (rainfall, runoff and soil moisture)
- Evaluate the prediction skill of the coupled WRF-Hydro model under extreme conditions.

4. Research design and methods

4.1. RO1: Investigate the teleconnections between global climate driving factors and seasonal and sub-seasonal rainfall variations over Northern Ethiopia

4.1.1. Introduction

The Horn of Africa rainy season is classified as a summer maximum rain to the north (JJAS) and bimodal rain season to the south with the boreal spring long season (MAM) and short rainy season October-November (Nicholson, 2014). As mentioned earlier, this study is, however, focusing on the northern part of Horn of Africa with long season-boreal summer (JJAS rainfall). This seasonal rainfall is largely governed by large-scale anomalies of ENSO (Table 4.1). As the climate in Northern Ethiopia is very complicated, for summer rainfall prediction, different studies have used different predictors from different regions of the Atlantic, Pacific and Indian oceans, and different regional and local atmospheric factors (Table 4.1). Besides, the local atmospheric circulations near East Africa, the Indian Ocean and the Atlantic ocean have significant roles (Korecha & Barnston, 2007). This indicates that the Ethiopian JJAS rainfall can reliably be forecasted by integrating the oceanic variables with that of the atmospheric factors.

Table 4.1: Summary of global SST regions and Zonal winds that have shown strong correspondence with the Northern Ethiopia JJAS rainfall. Where, CEI: Central Equatorial Indian Ocean Index, WIO: Western Indian Ocean, EIO: Easter Indian Ocean, Nino 3.4: ENSO average, ML-NWP: mid-latitude northwest Pacific, EEAI: Equatorial Easter Atlantic Ocean (Gulf of Guinea) and TAD: Tropical Atlantic Dipole.

S/n	Oceans	Regions	Area coverage	Reference
1	Indian ocean	CEI	0° - 15°S and 50°E-80°E	Degefu et al. (2017)
		WIO	10°S-10°N and 50°E-70°E	Gissila et al. (2004); Segele & Lamb (2005); Segele et al. (2015)
		EIO	10°S–0° and 90°E–110°E	Gissila et al. (2004)
		IOD	WIO-EIO	Degefu et al (2017); Camberlin (1997)
2	Pacific Ocean	Niño 3.4	5°N-5°S and 120°-170°W	Degefu et al. (2017); Diro et al. (2008, 2011a; 2011b);Gissila et al. (2004); Gleixner et al. (2017); Korecha & Barnston (2007); Nicholson (2014, 2015); Segele & Lamb (2005); Segele et al. (2009); Segele et al. (2015); Zaroug et al. (2014)
		ML-NWP	30 °-45 °N and 145 °-165 °W	Diro et al. (2008, 2011a; 2011b)
3	Atlantic Ocean	EEAI	5°N-25°N and 15°W-55°W	Degefu et al. (2017); Diro et al. (2008, 2011a; 2011b); Rowell (2013)
		TAD	(5°N-25°N and 15°W-55°W) - (0°–20°S and 10°W–30°W)	Degefu et al. (2017); Rowell (2013)
4	High Level wind	100-300hPa	30E-90 E and 0-15 N	Segele et al. (2015) and Gleixner et al. (2017) , Nicholson (2014) and Zeleke et al. (2013)
5	Lower level wind	550hPa, 850hPa and 1000 hPa	30E-90 E and 0-15 N	Segele et al. (2015) and Zeleke et al. (2013)

Therefore, in this study, the teleconnection of the seasonal and subseasonal JJAS rainfall variations with the global SST, and Zonal winds at a lower level (850-1000hPa) and upper level (100-300hPa) will be investigated. This approach is consistent with Nicholson (2014) and Segele et al. (2015) that the seasonal Ethiopian JJAS rainfall is associated with the slowly changing of SST anomalies through changes in regional and local atmospheric circulation.

Though, the MJO anomalies is strongly linked to intraseasonal (sub-seasonal) variations over tropical atmosphere (NASEM, 2016; Vitart et al, 2014; White et al., 2017), the MJO signals did not show good correspondence with the sub-seasonal JJAS rainfall variation over the Horn of Africa (Camberlin & Philippon, 2002; Zaitchik, 2017). This is due to the fact that the MJO signals are strong during the spring season.

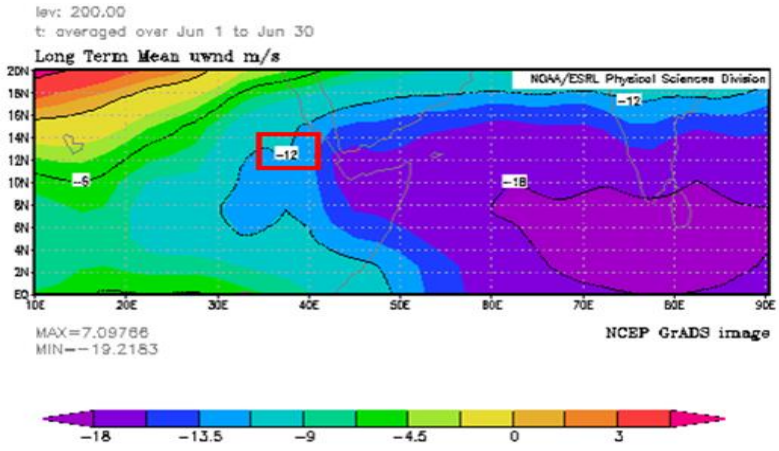

Figure 4.1. Daily average TEJ propagation (June 01-30, 2018) at geopotential height of 200hPa over the Horn of Africa. The study area is located in the red box. Source: Physical Sciences Division, Earth System Research Laboratory, NOAA, Boulder, Colorado, at http://www.esrl.noaa.gov/psd/.

Nevertheless, from the major atmospheric variables, the Northern Ethiopian seasonal and sub-seasonal JJAS rainfall variations have good correspondence with the intraseasonal TEJ fluctuations. For this reason, in combining with SST teleconnections, the mechanistic link of sub-seasonal JJAS rainfall variations to the intraseasonal TEJ variations will be investigated. The TEJ happens during the monsoon season(June-September) with intraseasonal timescale (30-60 days) variability. The TEJ occurs around 70^0E and propagates horizontally between 5°N and 15°N and 30°E to 90°E (Figure 4.1) and vertically between 70 hPa and 300 hPa (Sathiyamoorthy et al., 2007). Overall, this research will be aiming at answering the questions listed hereunder:

- What are the global SSTs that can be linked to the seasonal and sub-seasonal JJAS rainfall variations?
- What type the zonal winds are associated with the seasonal and sub-seasonal JJAS rainfall variations?
- Which one or what combination of oceanic-atmospheric variables are most strongly correlated with JJAS rainfall variations?

- Can integrated use of these ocean-atmospheric variables improve the rainfall predictions skills at seasonal and sub-seasonal timescales?

4.1.2. Data

4.1.2.1. Observed rainfall data

The temporal scope of the study depends on the data availability and, in general, it will initially cover a time length of 12 years (2009-2020). This time range is selected considering the station-based observed rainfall data in that the time series data available for most of the station is since 2009. The observed daily rainfall data for teleconnection, model validation and performance evaluation will be collected from meteorological stations, satellite-based, and measured (field survey) data. The observed daily rainfall data from 13 meteorological stations in and around the study area (Figure 4.6b) will be collected from Ethiopian NMA. The data availability varies from station to station and is not distributed uniformly across the catchment (Figure 4.6b).

To minimize errors due to the sparse distribution of the gauging stations, gridded based rainfall data will be used. This can be either from the areal precipitation of the existing rainfall stations using interpolation methods or satellite-based observation. The satellite-based observations can be from high spatial and temporal resolution station based algorithms such as the CHIRPS dataset from Climate Hazard Group database (ftp://ftp.chg.ucsb.edu/pub/org/chg/products/CHIRPS-2.0/) and/or from other analysed and reanalysed products such as ENACTS from NMA, ECMWF and UK Met office. The CHIRPS observed rainfall is at 0.05° spatial resolution and 6-hourly, daily and monthly temporal intervals. In areas with high topographic variations like East Africa (Funk et al., 2015), the dataset can reasonably represent the station-based rainfall observations (Dinku et al., 2018; Gebrechorkos et al., 2018; Kerandi et al., 2018). For simple comparisons, the areal precipitation from the in-situ observations and CHIRPS rainfall are presented in Figure 4.2. The graph indicates that the mean monthly averages from both data sources have good agreements.

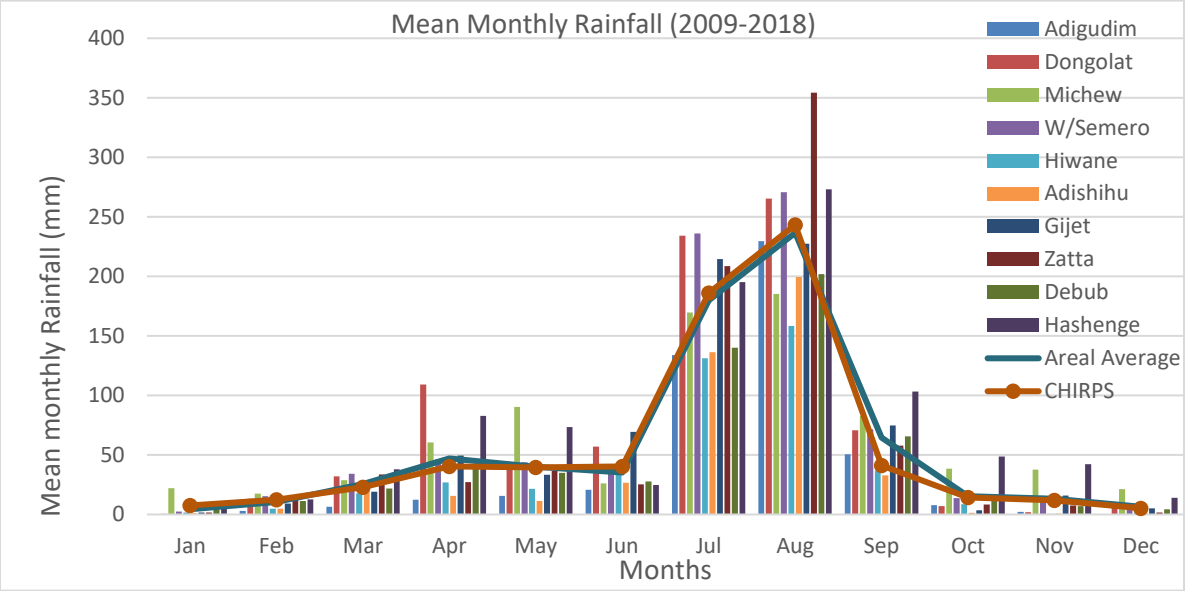

Figure 4.2: Mean monthly and areal mean monthly rainfall of the study area (2009-2018) from 10 stations as indicated in Figure 4.6b. and areal mean monthly rainfall from CHIRPS observations.

The advantage of the use of analysis or reanalysis data for model verification in situations where the conventional in-situ data are sparse has been illustrated by Warner (2011). However, such analysed and reanalysed daily rainfall data may require verifications from station-based observations as they are based on the coarser resolutions. In this study, for better use of in-situ rainfall observation, satellite-based observations will be compared with that of the station-based observations and will be corrected if necessary. Such reliable and accurate observed data is crucial because the accuracy of the model simulations will be measured relative to these observations.

4.1.2.2. Global SST and Zonal wind

For this study, mean monthly (MAM) global SSTs covering the time length of 2009 to present will be retrieved from IRI data Library: NOAA/Reyn_SmithOIv2/ database (NOAA OI.v2 SST) and at the website: http://iridl.ldeo.columbia.edu/SOURCES/.NOAA/.NCEP/.EMC/.CMB/.GLOBAL/.Reyn_SmithOIv2/.monthly/.sst/. The NOAA OI.v2 SST monthly fields are constructed based on linear interpolation of the weekly optimum interpolation (OI) version 2 fields to daily fields then averaging the daily values over a month (Reynolds et al., 2002). It is mainly based on in-situ sea surface observations (using ships and buoys) and satellite observations from Advanced High-Resolution Radiometer (AVHRR). The global SST data that covers 180W to180E longitude and 60°N-60°S latitude with 1° x1° horizontal resolutions centred at 0.5° will be obtained. For the specific climate indices (Table 4.1) mean monthly SST will be retrieved from NOAA-PSD: Climate Indices/Monthly Atmospheric and Ocean Time Series (website: https://www.esrl.noaa.gov/psd/data/climateindices/list/). Mean monthly (May-September) zonal wind levels from geographical location 30°E-70°E and 0-20°N (for lower-level wind at geopotential of 550, 850 and 1000hPa, and for upper-level winds at geopotential height of 100, 200, and 300hPa) will also be retrieved from NCEP-DOE Reanalysis 2 data provided by the NOAA/OAR/ESRL PSD, Boulder, Colorado, USA, at Website: https://www.esrl.noaa.gov/psd/).

4.1.3. Selection of ocean-atmospheric teleconnections

Possible ocean-atmospheric variables that link to the Ethiopian JJAS rainfall will be selected based on two steps. First, detail investigation on a large set of teleconnection candidates such as SSTs from different regions of the Pacific, Atlantic, and Indian ocean and Zonal wind at five pressure levels (100hPa, 200hPa, 300hPa, 550hPa, 850hPa and 1000Pha) will be conducted. For better understand, three sets of composites based on the precipitation characteristics (i.e., for the dry, normal and wet conditions) will be used. Then, a correlation map between JJAS Northern Ethiopia rainfall and the global SST at every grid point with lag time 1-3 months (MAM) and with the Zonal winds with lead time of five months (one month in advance from previous season i.e., May and four months in contemporaneous season (June-September) will be constructed.

From these maps, based on correlation coefficients and visual inspection, areas that show a strong correlation will be selected as potential teleconnection candidates. For instance, a correlation map (Figure 4.3) between Northern Ethiopia July rainfall and monthly average global SST of May (2009-2017) shows that the July rainfall over Northern Ethiopia is negatively correlated with Equatorial Eastern Atlantic Ocean (blue box) and positively correlated with Northwest Indian ocean (green box).

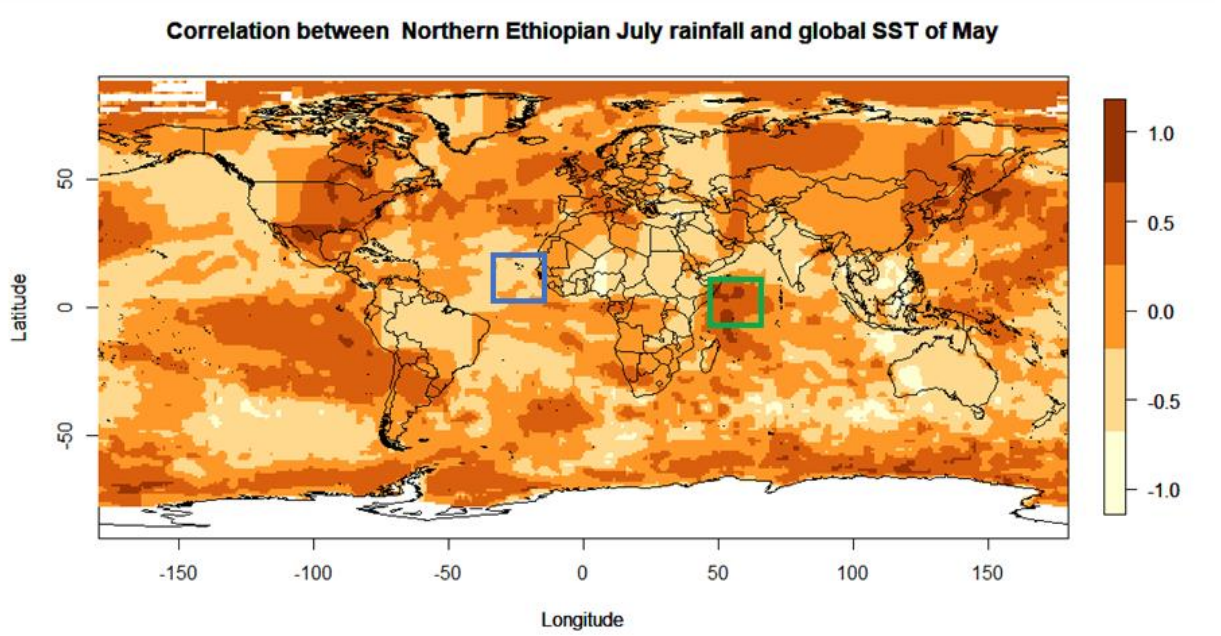

Figure 4.3: Correlation map between July rainfall over Northern Ethiopia (38.9°-39.7° N and 12.6°-13.3°E) and mean monthly global SST of May. The blue (Equatorial Eastern Atlantic Ocean) and green box (Northwest Indian ocean) represent oceanic regions that indicate negative and positive correlations, respectively.

In a wide range of correlation maps, especially in global SST regions, a number of candidates can be expected. To minimize these candidates, Sea surface regions which are very close to the climate indices regions (Table 4.1) that show a strong correlation at significance level 0.05 will be selected. Then a sensitivity test of the regression to each predictor will be employed (Nicholson, 2014). From the sensitivity analysis, predictors that are highly sensitive will be selected as key variables. Once the predictor candidates are properly identified, empirically linear relationships will be developed (Appendix: section 8.1.2). This is in agreement with Chen & Georgakakos (2015) that If the oceanic-atmospheric variables are accurately investigated, establishing an empirical predictor–predictand relationship is a simple and robust tool for statistical predictions.

During the selection of an appropriate teleconnection candidate, collinearity and overfitting might happen due to the dependency between candidate predictors (Diro et al., 2008; Nicholson, 2014). To avoid multicollinearity and overfitting, each potential candidate will be regressed against the other predictors. From these regressions tests, the best predictors will be selected based on the Variance Inflation Factor (VIF) which is given by *Equ. 4.1* (Diro et al., 2008).

$$VIF = \frac{1}{1 - {R_i}^2} \dots\dots\dots\dots\dots\dots\dots (Equ. 4.1)$$

Where ${R_i}^2$ is the regression coefficient of the *i*th candidate. A candidate that shows more than 10 % of VIF, can be lower to 4% (Chen & Georgakakos, 2015), will be eliminated from the final selections.

4.1.4. Sensitivity and accuracy assessment

The sensitivity of the ocean-atmospheric variables and accuracy of the regression model will be assessed using statistical methods (Appendix 8.1) such as correlation coefficient, Bias (Mean Error), Root Mean Square Error (RMSE), Mean Absolute Error (MAE) and skill score (SS). The use of these techniques is consistent with recent studies (Abdelwares et al., 2017; Kerandi et al., 2017; Pohl et al., 2011) and recommendations (Warner, 2011).

Last but not least, the overall methodological framework for RO1 is summarized in Figure 4.4 hereunder.

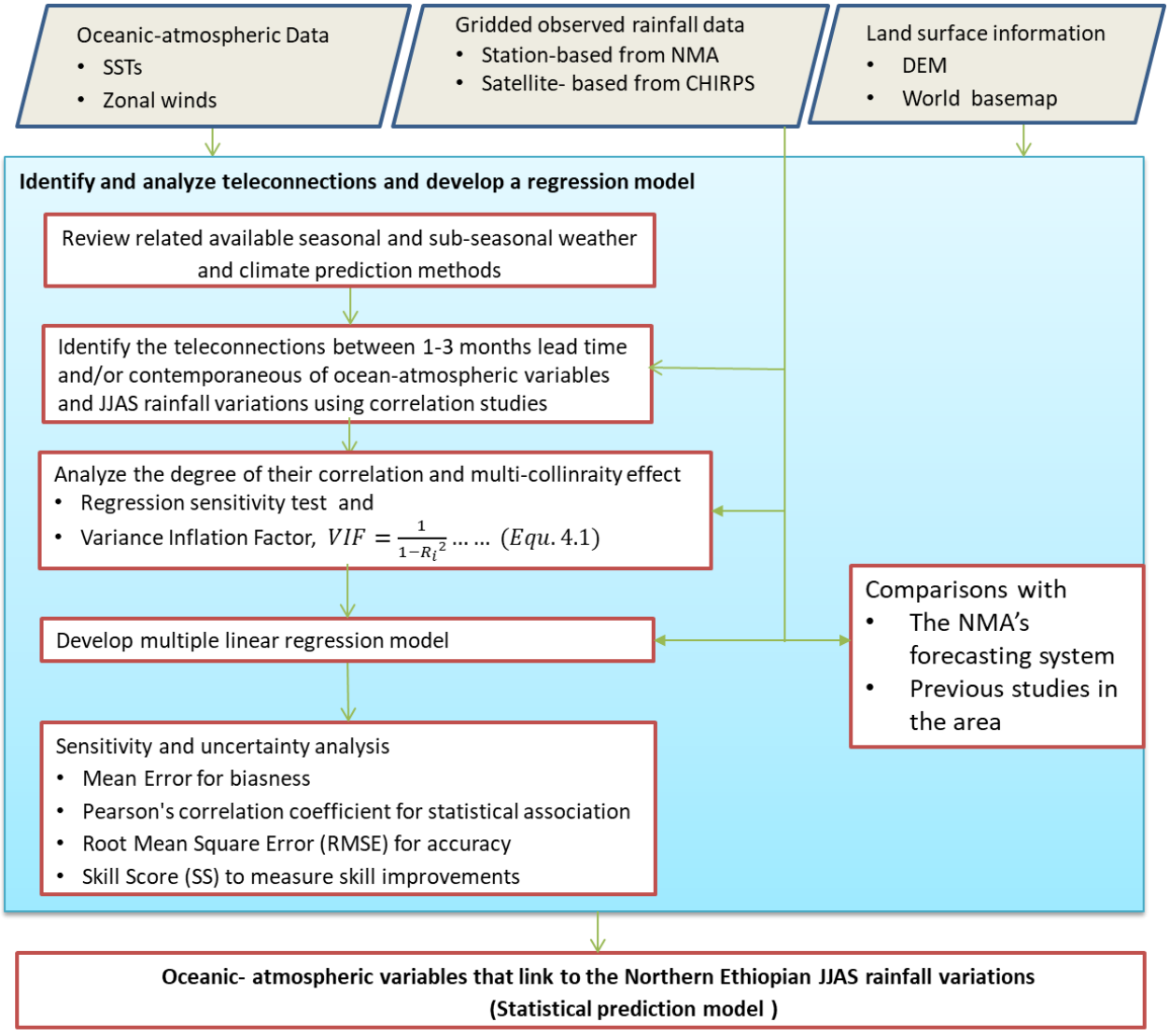

Figure 4.4: Schematic workflow to identify oceanic atmospheric factors that link with the JJAA rainfall variations and develop empirical relationships. Where, NMA: National Meteorological Agency, SST: Sea Surface Temperature, and DEM: Digital Elevation Model at high resolution (30 meters or higher)

4.2. RO2: Customize the WRF model as a regional climate model for seasonal and sub-seasonal rainfall prediction over Northern Ethiopia

4.2.1 Model selection

Reliable and accurate rainfall prediction can be carried out by understanding the interaction between the ocean-atmosphere and thus with the land surfaces (White et al., 2017). The use of joint ocean-atmospheric variables that show a strong statistical link in reproducing the weather and climate components requires the employing of numerical models. The choice of the NWP model depends on the demands for appreciating the regional and local variations (Warner, 2011). In line with, in Ethiopian, the summer rainfall is strongly linked to both remotely oceanic parameters (SST) and regional and local atmospheric circulations. This implies that the use of NWP models that can couple the ocean with the regional and local atmosphere variables for reliable rainfall predictions is essential. Globally, there are weather/climate prediction models that are effective in simulating weather and climate variables at various timescales and spatial resolutions. For instance, the GFS (GFS, 2018), ECMWF (Olaniyan et al., 2018; Stockdale et al., 2018) and the CFSV2 (Saha et al., 2014; Siegmund et al., 2015; Tian et al., 2017) models are among the widely used GCMs for seasonal and subseasonal rainfall prediction. As these forecasts are at global scale, dynamically downscaling into regional and local scales using RCMs is however becoming a common practice (Simon, 2008; Tang et al., 2016; Vecchi et al., 2011). This method of downscaling may provide full sets of the microphysics at higher resolutions to regional numerical models (Tang et al., 2016) so that weather and climates can be reliably forecasted at finer scales.

Thus, for this study, the next generation mesoscale WRF model is chosen as a regional climate model for dynamically downscaling the seasonal and subseasonal forecast from global prediction models. The model is selected due to (1) its ability to address smaller atmospheric scales (regional and synoptic scales), (2) it is dynamically coupling the ocean-atmosphere-land surfaces (3) it capacitates the research to operation developments (e.g. Ethiopian NMA uses the WRF model for 72 hours of operational forecasts), (4) it provides extension facilities such as WRF-Hydro to investigate the atmosphere-terrestrial relationships; and (5) Moreover, due to its high-level numerical accuracy and scalable regional modelling properties (Powers et al., 2017; Skamarock et al., 2008). The use of WRF model as RCM is consistent with recent studies in several regions of the world, for example, in East and West Africa (Argent et al., 2015; Kerandi et al., 2018; Naabil et al., 2017; Siegmund et al., 2015; Yao et al., 2017).

However, in areas with a complex topography and climate system, like Northern Ethiopia (Nicholson, 2014), forcing the WRF model for reliable and accurate prediction requires accurate representations of the oceanic-atmospheric-land surface variables (Flaounas et al., 2012; Jee & Kim, 2017; Jung et al., 2012; Senatore et al., 2014; Song et al., 2009). This is due to the fact that RCMs are weak to represent the reality due to insufficient resolution of inputs provided to the models (Carvalho et al., 2012; Ntwali et al., 2016). More noticeably, the Ethiopian JJAS rainfall distribution, both spatially and temporally, is largely influenced by the complex orography (Enyew & Steeneveld, 2014; Korecha & Barnston, 2007). In the WRF model, the sensitivity of the model to the major initial and boundary conditions such as meteorological inputs and topographic features in reproducing JJAS rainfall over Northern Ethiopia can be assessed through three approaches: (1) considering sufficient horizontal resolution, (2) choosing appropriate vertical coordination system and (3) enhancing the model inputs/improving the representations of the model inputs.

4.2.2. The WRF model

For this research work, the Advanced Research WRF model (WRF-ARW) Version 4 (Skamarock et al., 2008) will be used. The WRF-ARWS Version 4 is a non-hydrostatic, mesoscale NWP and atmospheric simulation system. It is a community-based model that has been released since June 2018 by the National Centre for Atmospheric Research (NCAR). The model is designed with a flexible code to be utilized for several purposes of research and operational predictions (Powers et al., 2017). Despite its demand for a high computing machine, it's portable and efficient on available parallel computing platforms. The model is capable to provide a wide range of earth system prediction applications across different spatial and temporal scales (Skamarock et al., 2008). It offers a quite large number of different physical schemes that can be combined in any way and optimized to any region of interest. Details about these physical parametrizations and their characteristics are found in the WRF model description document (Skamarock et al., 2008). The overall schematic workflow of the WRF model for this project is presented in Figure 4.5. The WRF model architecture consists of three sub-process (Skamarock et al., 2008): (1) WRF Preprocessing System (WPS-defining model domains), (2) WRF-ARW core processing and (3) WRF Post-processing System (WFP- analysis and visualizing of the WRF model outputs).

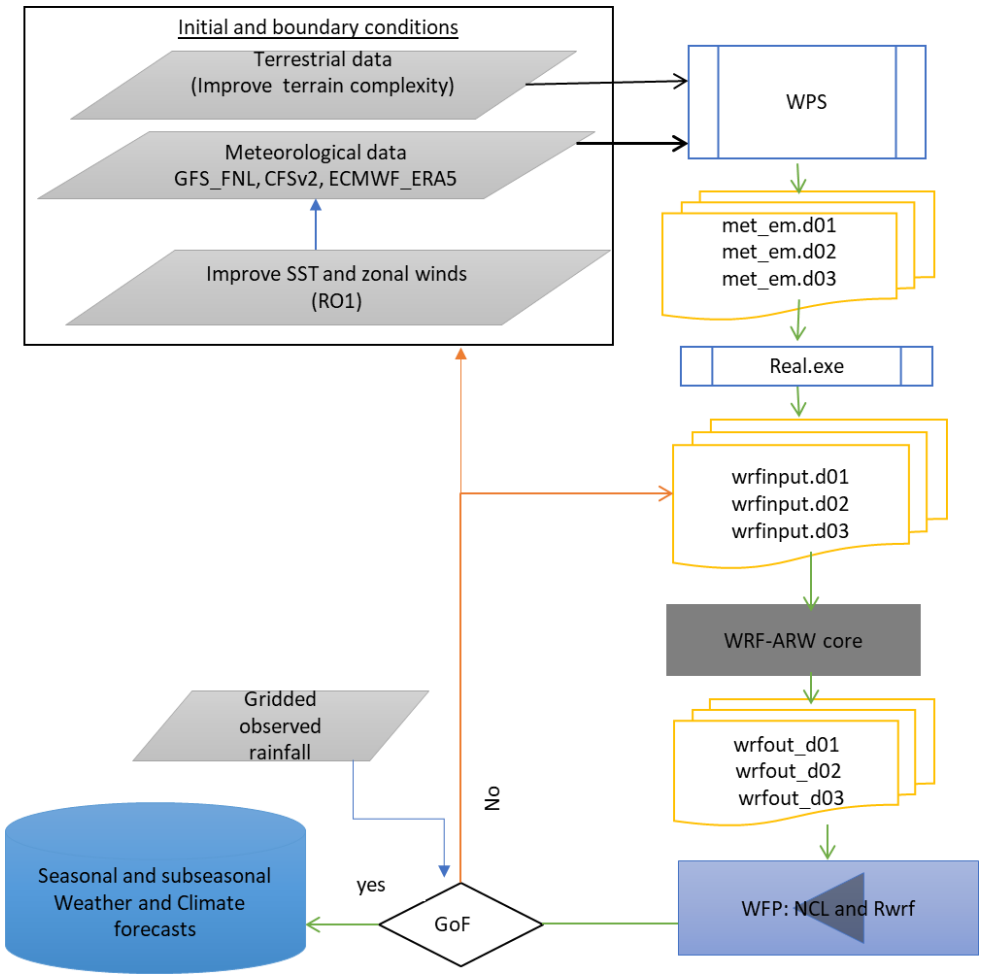

Figure 4.5: Schematic methodological flowchart of the WRF-ARW modelling System for numerical rainfall predictions. Where, WPS: WRF pre-processing system, WFP; WRF post-processing, NCL: NCAR Command Language, Rwrf: R package for WRF post-processing and GoF: Goodness-of-Fit test

4.2.3. Model Configuration

This study will be conducted in the upper Tekeze river basin, specifically in Zamra catchment, Northern Ethiopia. The study site is found in a region between 12.62^0-13.30^0N and 38.92^0-39.62^0E and covers an area of around 3500 km^2 (Figure 4.6b). The catchment consists of four sub-basins and is situated in the highlands of Northern Ethiopia and altitude varies from 1134- 3948 m.a.s.l. It is the main tributary of the upper Tekeze basin and particularly to Tekeze Dam. The annual rainfall (2009-2018) of the study area varies spatially (Figure 4.2) and ranges from around 420 mm in the lowlands to around 900 mm on the highlands. The mean monthly temperature also varies from 13^{o}c to 28^{o}c. The study area is selected based on data availability, access for research, active water resources infrastructures, vulnerability to drought and interest of the EENSAT project.

The domain configurations for the WRF model for nesting from the outer domains to inner domains is shown in Figure 4.6a. The procedures for WRF domain size configurations vary from researcher to researcher and, in general, there is no rule of thumb (Jee & Kim, 2017). However, most researchers including that of the model description (Skamarock et al., 2008) suggested a 1:3 domain ratio between the outer to the inner domains. For this study, three two-way nest domains with a ratio of 1:3 centred at 13 Northing and 39.4 Easting using Mercator map projection (Figure 4.6a) are established.

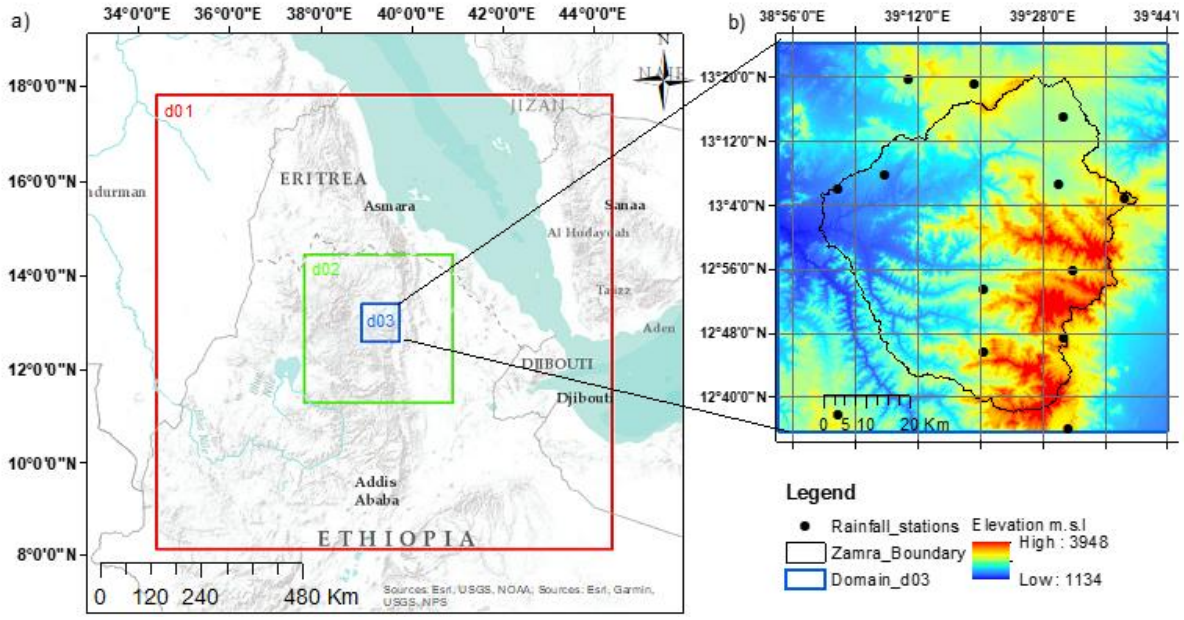

Figure 4.6: Horn of Africa map that shows the model configuration domains (a): the red box represents the parent domain (d01), while the nesting domain with green box and the blue boxes show the inner domains d02 and d03, respectively and (b) study area map with topography (the DEM) and rain gauge distribution across domain_d03.

The parent domain (d01), domain (d02) and inner domain (d03) are defined with a horizontal resolution of 27 km, 9 km and 3 km, and 41X41, 40X40 and 31X31 grid points east-west and north-south directions, respectively. The higher horizontal resolution of the outer domain is chosen in agreement with the horizontal resolution of the selected GCM products. In addition, it has been reported (Jee & Kim, 2017; Kerandi et al., 2017) that the skill of the WRF model predictions increases with increase outer domain

horizontal resolution. The ratio of 1:3 helps to nest the initial and boundary conditions from the coarser parent domain smoothly to the inner domains. This smoother transition is an essential procedure to prevent the propagation of uncertainties and numerical instabilities from the border into the centre of the domain (Jee & Kim, 2017). In addition, to avoid the uncertainties during driving initial and boundary conditions from GCM analysis and/or reanalysis outputs, a grid-based nudging technique will be applied (Pérez et al., 2014). The nudging techniques adjust the difference between a pair of states (observed and forecasted). In this case, only the parent domain is nudged to let the inner domains create their own structure at finer resolutions. The outputs from the three domains will be compared to each other and with that of the observed rainfalls.

Verifying vertical resolution as a key parameter in given domain sizes has a significant contribution to the prediction skill of the WRF model (Pohl et al., 2011). The vertical resolutions refer to the number of vertical levels that can vertically be interpolated to the model domains. Warner (2011) emphasized that the choice of vertical resolution directly associated with the size of the domain configurations. For this study, two vertical resolution: (1) the WRF model default values i.e., 28 vertical layers with 5000 Pa top atmospheric pressure, and (2), as per the recommendations of Skamarock et al. (2008), for a 27-km horizontal resolution, 51 vertical layers with the top atmospheric pressure of 1000 Pa will be adapted.

4.2.4. Data

For this research, daily time series of in-situ rainfall observations (from section 4.1.2.1.), initial and boundary conditions, forcing initials such as SST and Zonal winds (from section 4.1) will be collected for the time range of 2015-2020. Such a short period of data is required because, for a large group of experiments, it demands high computing resources. The year 2015 is selected considering the fact that this has been a drought-affected year over Northern Ethiopia (Funk et al., 2016).

4.2.4.1 Forcing initials: initial and boundary conditions

For this study, forcing initials and boundary conditions: the highest resolution (30s) geographic data form WRF Users Page (Website: http://www2.mmm.ucar.edu/wrf/users/) and the ECMWF-ERA5 reanalysis meteorological inputs from ECMWF climate data store (website: https://cds.climate.copernicus.eu/) will be retrieved. The ECMWF-ERA5 data is at 31 km spatial resolution and 6-hourly temporal intervals. The dataset is produced using 62 km horizontal resolution 10-member 4DVar data assimilation product with 137 hybrid sigma-pressure levels, up to 0.01 hPa (ECMWF, 2017). The database is among the widely exploited databases in the world and particularly in East Africa (Abdelwares et al., 2017; Argent et al., 2015; Diro et al., 2012; Kerandi et al., 2018; Kerandi et al., 2017; Pohl et al., 2011; Srivastava et al., 2015; Yao et al., 2017). Hence, the use of ECWMF-ERA5 reanalysis as forcing initial and boundary condition in this study is consistent with the studies over East Africa.

4.2.5. Research design and experiments

This study proposes three major research designs consisting of different specific experiments in order to properly customize a framework of the WRF model configurations for Northern Ethiopia JJAS rainfall predictions. These are: (1) optimization of physical options, (2) optimization of forcing initials and lateral boundary conditions and (3) sensitivity analysis of SST, Zonal winds and terrestrial complexity. These experiments are mainly to answer the following questions:

I. Can customizing the WRF model as a regional climate model improve the seasonal and subseasonal rainfall predictions over Northern Ethiopia?
II. Can the optimization of forcing initials from different global weather and climate prediction datasets improve the prediction skill of the WRF model over Northern Ethiopia?
III. If the regionalized WRF model is forced by global and regional climate driving factors that link to the Northern Ethiopia JJAS rainfall, will its prediction skill be improved?
IV. Can enhance the terrain representations of the WRF model improves the simulation skill of the model under complex topography, like Northern Ethiopia?
V. What are the sensitive/optimal parameters of the WRF model for seasonal and sub-seasonal JJAS rainfall predictions?

4.2.5.1 Customization physical options

The WRF model contains a quite large number of parameters. To identify optimal physical parameters that enable reasonable seasonal and sub-seasonal rainfall forecasts, customization of the WRF model in a comprehensive approach is crucial (Argent et al., 2015). In this study, the optimization will be focused mainly on the major physical option: (1) Cumulus conservation (CU), (2) Microphysics (MP), (3) Planetary Boundary Layer (PBL), (4) Long-wave radiation (LW), (5) shortwave radiation (SW) that potentially affect the rainfall characteristics (Abdelwares et al., 2017; Argent et al., 2015; Pohl et al., 2011; Siegmund et al., 2015). Detail descriptions of these parametrizations are available in the WRF model version 4 document (Skamarock et al., 2008). The model is flexible with different options depending on the demand for the domain configuration. Nevertheless, parameterization of the physical options of the WRF model into local scales is among the challenging task of the RCM (Abdelwares et al., 2017). In East Africa, there were some efforts to customize the WRF model as a regional climate simulation model (Abdelwares et al., 2017; Pohl et al., 2011). Despite the complex climate system and terrain characteristics (Diro et al., 2012; Nicholson, 2014), they have concluded that the WRF model can be potentially useful as RCM over East Africa. Nevertheless, these generalizations are based on (1) large domains, and (2) most of the studies were focused on the spring season (March to May rainfall). For example, the WRF model customizes study for seasonal climate simulation (Argent et al., 2015) over the Lake Victoria basin have confirmed that the local findings did not agree with the regional recommendations. Even the recent result from customization of the WRF model over the northeast part of East Africa (Abdelwares et al., 2017) varies from that of Pohl et al. (2011). This indicates that customization of the WRF model parametrization into more local conditions are required.

Therefore, this research work is set-out to customize optimal combinations of the WRF model parametrizations that can enable to regenerate JJAS rainfall over the Horn of Africa. For this experiment, three parameter schemes from each physical option (Table 4.2) are selected. The selection was carried out based on previous sensitivity studies for arid and semiarid regions, particularly for West and East Africa (Abdelwares et al., 2017; Argent et al., 2015; Noble et al., 2017; Otieno, Mutemi, Opijah, Ogallo, & Omondi, 2018; Pohl et al., 2011; Ramarohetra et al., 2015; Yao et al., 2017) and the description of the schemes related to the specific location of the domains. In addition, the WRF Model contains two sources of land use classifications: the U.S. Geological Survey (USGS) based on 24 classes and the Moderate Resolution Imaging Spectroradiometer (MODIS) with 20 land use classes (Skamarock et al., 2008). It has been suggested that for East African (Kerandi et al. 2017), for West Africa (Ramarohetra et al., 2015) and particularly for Ethiopian rainfall (Abdelwares et al., 2017; Pohl et al., 2011), the WRF configuration with

MODIS land use classification has shown superior simulation skill over that of the USGS. The MODIS model is also the default land use model of the WRF model. Herein, the MODIS land use with Noah land surface modelling will be used in agreement with these recent findings. The experimental designs to customize optimal WRF model physical parametrizations for Horn of Africa climate system is presented in Table 4.3 (Exp.1-Exp 5).

Table 4.2. summary of selected physical options, parameter schemes, and their Model_ID. Adapted from Skamarock et al., (2008)

Physics options	Model _ID	Scheme	Reference
CU	1	Kain-Fritsch (KF)	Kain (2004)
	2	Betts Miller Janjic (BMJ)	Janjic, 1994, 2000
	3	Grell-Freitas (GF)	Grell et al. (2013)
MP	2	Lin et al. scheme (Lin)	Lin et al. (1983)
	6	WRF Single-Moment 6-Class scheme (WSM6)	Hong and Lim (2006)
	10	Morrison double -moment scheme (Morrison)	Morrison et al. (2009)
PBL	1	Yonsei University (YSU)	Hong et al. (2006)
	2	Mellor-Yamada-Janiic (MYJ)	Janice (1994)
	7	Asymmetrical Convective Model version 2 (ACM2)	Pleim (2007)
LW	1	Rapid Radiative Transfer Model (RRTM)	Mlawer et al. (1997)
	14	Improved RRTM for global climate applications (RRTMG-K)	Baek (2017)
	3	NCAR Community Atmosphere Model (CAM)	Collins et al. (2004)
SW	1	Dudhia	Dudhia (1989)
	2	New Goddard (Goddard)	Chou and Suarez (1994)
	3	CAM	Collins et al. (2004)

4.2.5.2 Model initializations

The choice of an appropriate forcing GCM products has a strong impact on the regional and local simulated climate variables (Abdelwares et al., 2017), especially in areas with high terrain complexities (GFS, 2018). Hence, evaluating the WRF model performance in relating to the initial and lateral boundary conditions that dynamically downscaling from relevant but different GCM databases is crucial (Pohl et al., 2011; Yao et al., 2017). Herein, the performance of the WRF model to reproduce the observed rainfall using initial and boundary condition from the GFS-FNL and CFSv2 6-hourly forecasts will be assessed. The GFS-FNL and CFSv2 6-hourly forecast will be retrieved from the NCAR Research Data archive (Website: http://www2.mmm.ucar.edu/wrf/users/download/). The GFS-FNL data is an operational global analysis and forecast data at 0.25^{o} horizontal resolution, available every six hours and updated daily. The GFS-FNL 6-hourly forecast is a product of the GFS model using continuously collected observational data from the Global Telecommunications System (GTS) with the global data assimilation system (NCEP, 2015). The CFSv2 dataset is also 6-hourly forecasts of the pressure and surface/nearly surface atmospheric data at 0.2^{o} horizontal resolutions(Saha et al., 2011).

Table 4.3: Available GRIB Datasets from NCAR for WRF Model. Adapted from(NCAR, 2018).

s/n	Dataset	Spatial Resolution	Temporal Resolution	Temporal Availability
1	GFS-FNL	0.25^{0}	6-hr	2015-07-08 to current
2	CFSv2	0.2^{0}	6-hr	2015-01-01 to current

These GCM products are chosen because (1) they produce global weather/climate forecasts at high spatial (less than 0.25^{o}) and temporal resolutions (less than or equal to 6-hours interval); (2) they are capable in providing initial and boundary conditions at seasonal and sub-seasonal timescales (Olaniyan et al., 2018; Tian et al., 2017; Frederic Vitart et al., 2012); (3) good in reproducing regional climate system in Africa and particularly East Africa (Gleixner et al., 2017); (4) their datasets is in GRIB2 format for which their forecasts, analysis and reanalysis data can be directly utilized by the WRF model (NCAR, 2018); and (5) in agreement with previous studies (Abdelwares et al., 2017; Diro et al., 2012; Gleixner et al., 2017; Pohl et al., 2011) for comparisons of the research outputs.

4.2.5.3 **Sensitivity of SST, zonal winds and terrain complexity**

Experiment 1: *improve horizontal resolution and vertical coordinate system*

Recent studies (Carvalho et al., 2012; Enyew & Steeneveld, 2014; Ntwali et al., 2016) have suggested that improving horizontal and vertical resolutions; smoothing the elevation gap between model and the reality and coupling with the best surface level, PBL and LSM schemes can improve the simulation skill of the WRF model. Herein, one additional domain configurations (Figure 4.7a) that represents two-way nesting between parent domain (d01) with 27-km horizontal resolution that covers sufficient area which includes the seas surfaces such as the western Indian Ocean and the Red Sea, and three inner domain (d02) with 9-km horizontal resolution for regional simulation (Horn of Africa), domain_d03 with 3-km horizontal resolution for Northern Ethiopia simulations and domain_do4 with 1-km for the upper Tekeze basin predictions will be established. In case of the vertical coordination system, the model will be forced with two options: (1) with terrain-following coordinate system and (2) Hybrid vertical coordinate system (i.e., the details: Skamarock et al., 2008). With these experiments, representativeness of SST, Zonal winds and terrain complexity and thus the prediction skill of the model will be assessed.

Experiment 2: *improve the representations of the major ocean-atmospheric inputs*

The oceanic variables such as the SST anomalies are an important variable to better understand interactions between the ocean and the atmospheric circulations (Reynolds & Chelton, 2010; Song et al., 2009). Song et al. (2009) have emphasized that the characteristics of atmospheric circulation such as wind speed, direction, wind curl, and others are linearly associated with SST characteristics. This has been confirmed by Jee & Kim (2017) and Song et al. (2009) in that the sources of SSTs and their resolution have a significant impact on the simulation of the atmospheric variables. In this study, to improve the model SST representations, enhanced SST fields will be ingested to the WRF environment. This enhancement will be independent of the forcing initials from the GCM products. Herein, a daily time series of SST from the WRF model will be compared with daily SST from sources with high spatial resolutions such as NOAA Optimum Interpolation SST (OISST) version2 (website: https://www.ncdc.noaa.gov/oisst). The comparison will be done by employing GIS-based external pre-processing tools using resampling with the nearest neighbour techniques (Senatore et al., 2014). Next, the new SST grids will be masked with the model defined SST grid points and ingested to the WRF lower boundary condition files. In addition, a sensitivity of the SST in reproducing JJAS rainfall by shifting the lag time and changing the SST by the values +/- equivalent to SST anomalies from the best teleconnections (RO1) will be assessed. Using similar steps, the sensitivity of the zonal winds (U-wind) will be examined. Then the ordinary steps of the WRF model processes will be followed and its degree of improvement will be assessed.

Experiment 3: *improve the static geographic inputs*

Using the same method, as described for the SST enhancement above, ancillary data such as the land cover, topography and soil type properties of the WRF model will be evaluated in relation to the real terrain characteristics of the domains. Then they will be improved to the level that can represent the reality of the model domains. For example, the current highest resolution of the WRF model (30-second) geographical inputs represent a topography (Figure 4.7c) with significant elevation deviations. The difference ranges from +77.27m up to -581m at the lower elevation and the mountainous terrain, respectively. This indicates that improving the representation of the topography may play a significant role in the accuracy of numerical hydrometeorological simulations (Carvalho et al., 2012; Flaounas et al., 2012).

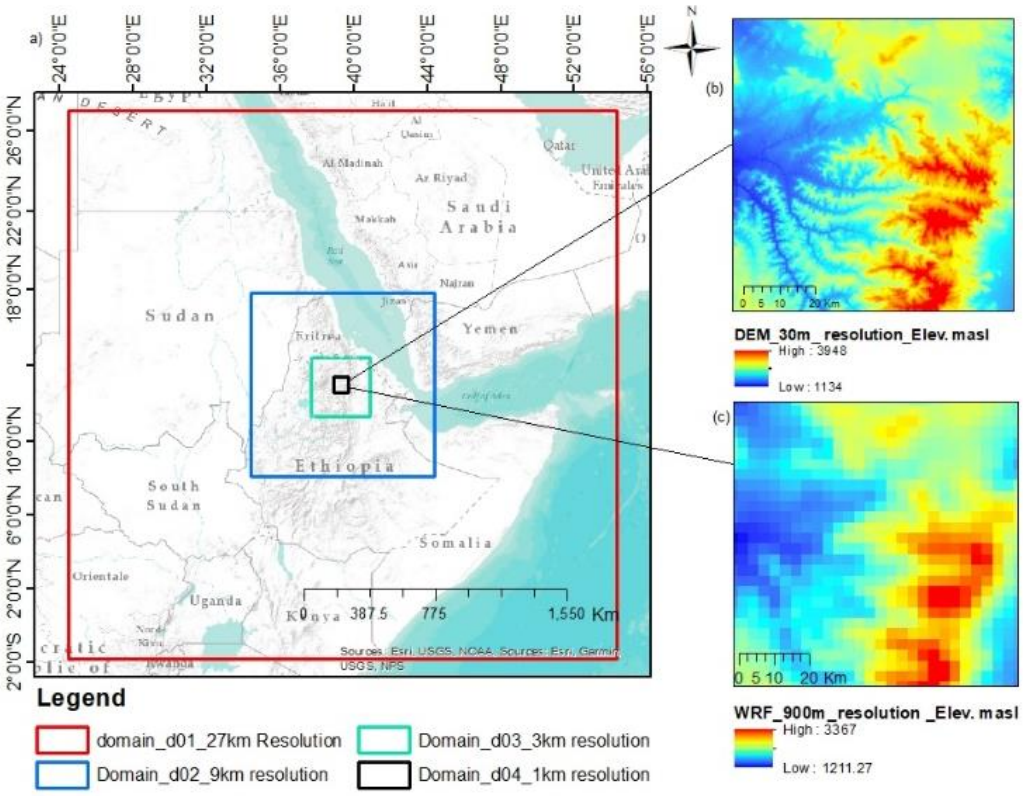

Figure 4.7: WRF domain configurations for sensitivity analysis of horizontal resolution (improved up to 1km resolution- domain_04 and large area coverages (domain_d01) (a) and a comparison of topographic representations from Digital Elevation Model (DEM) at 30-meter horizontal resolution (b) with the WRF Model at 30-second horizontal resolution (c).

4.2.6. **Model runs**

A series of simulations will be executed for the time length of four months: June- September 2015-2019. This simulation period is selected considering the demand for computing resources and time. The simulation will be initialized on April 01 and integrates on September 30, including 2 months (April and May) spin-up period to let the model adjust to initial conditions. Due to a large number of parameter combinations, the customization of the physical options will be conducted based on step-wise evaluations

(Pohl et al., 2011; Yucel et al., 2015). This implies when a single scheme is tested all other settings will be retained at a model control. The model control refers to the model default values and recommended model parameters from previous studies such as the KF for the CU (Otieno et al., 2018; Pohl et al., 2011); CAM for the LW and SW radiations and the MYJ for the PBL (Abdelwares et al., 2017); the WSM6 for MP and the MODIS-Noah for the LSM (Abdelwares et al., 2017; Kerandi et al., 2017; Pohl et al., 2011). A total of 28 WRF configurations for four/five years (considering the year of 2015 for the drought year, 2016 and 2017 for normal years and 2018 for a wet year) will be performed (see Table 4.3).

4.2.7. Method of analyses and performance evaluation

The model output from each run will be analysed and visualized using WRF post-processing tools such as NCL (NCL, 2018) and the R-packages. The model simulated rainfalls will be analysed at two temporal scales. For the sub-seasonal forecasts, the daily simulations that range from 10 to 60 days or weakly averages will be considered. Whereas for the seasonal prediction, a monthly and seasonal averages of simulated JJAS rainfall will be analysed. For continues variables like seasonal and sub-seasonal rainfall forecasts (Warner, 2011), the performance of the WRF model configurations will be assessed using three statistical metrics: (1) the accuracy indices (Appendix: section 8.1.3), (2) skill score (Appendix: section 8.1.4) and (3) correlation coefficients (section 8.1.1). The assessment will be carried out by comparing the model simulations with that of in-situ (satellite based) rainfall observations. In addition, the Taylor diagrams (Taylor, 2001) will be employed to visualize the strength and weakens of different WRF configurations in reproducing the observed rainfalls. These statistical methods are consistent with related studies(Abdelwares et al., 2017; Andrys, Lyons, & Kala, 2015; Hoedjes et al., 2014; Iguchi et al., 2017; Li, Li, & Jin, 2014; Noble et al., 2017).

Table 4.3: Summary of the WRF model configurations and experimental designs. Where, Exp. represents each experiment and the number in the brackets E.g., (3) indicates the number of runs per experiment

Experiment	Physical parametrization			Land use	Forcing GCM	Vertical layer (VL)	Domain size (Km)
	Physical options	Selected schemes	Controlled schemes				
Exp. 1 (2)	CU	• BMJ • GFl	PBL: MYJ MP: WSM6 LW: CAM SW: CAM LSM: Noah	MODIS	ECMWF-ERA5	28 & HVC	d01:27 d02:9 do3:3
Exp. 2 (3)	MP	• Lin • Morrison	CU: Exp. 1 PBL: MYJ LW: CAM SW: CAM LSM: Noah	MODIS			
Exp. 3 (3)	PBL	• YSU • ACM2	CU: Exp. 1 MP: Exp. 2 LW: CAM SW: CAM LSM: Noah	MODIS			
Exp. 4 (3)	LW	• RRTM • RRTMG_K •	CU: Exp. 1 MP: Exp. 2 PBL: Exp.3 SW: CAM LSM: Noah	MODIS			
Exp. 5 (3)	SW	• Dudhia • Goddard	CU: Exp. 1 MP: Exp. 2 PBL: Exp.3 LW: Exp. 4 LSM: Noah	MODIS			
Exp. 6 (2)			CU: EXP. 1 MP: Exp. 2 PBL: EXP. 3 LW: Exp. 4 SW: Exp. 5 LSM: Noah	MODIS	GFS-FNL CFsv2		
Exp. 7 (2)			CU: Exp. 1 MP: Exp. 2 PBL: Exp. 3 LW: Exp. 4 SW: Exp. 5 LSM: Noah	MODIS	Exp:6	50 and TFC	
Exp.8 (3)			horizontal resolutions			Exp.7	d01:27 d02:9 do3:3 d04:1
Exp .9 (3)			SST (Pacific, Atlantic, Indian)				
Exp. 10 (2)			Zonal wind (UW, LW)				
Exp 11 (1)			Orographic impact				

4.3. RO3: Couple the atmospheric to a terrestrial model using WRF-Hydro for seasonal and sub-seasonal streamflow predictions of the Upper Tekeze river basin in Northern Ethiopia

In arid and semiarid environments with highly variable climate systems like Northern Ethiopia, understanding the hydrometeorological variables ahead of time requires a detailed investigation of the ocean-atmospheric-land surface interactions. The issue of ocean-atmospheric interaction can be dealt with applying regional climate models such as the WRF model (Kerandi et al., 2017). However, investigations related to ocean-atmospheric-terrestrial interactions in a specific area of interest require long-term in-situ observation of the water balance components (such as rainfall, runoff and soil moisture). Nevertheless, in areas with data scarcity, the ocean-atmosphere-terrestrial interaction can be studied by using the RCMs in combination with hydrological models (Kerandi et al., 2018). The use of joint atmospheric-hydrological models such as WRF-Hydro enhances the level of understanding of the atmospheric-terrestrial process by nesting global scale information to the regional and local scales through the regional atmospheric models (Gochis et al., 2018). The nesting can be either one-way or two-way coupling. The one-way nesting is the simplest one which provides information only from the atmospheric model to the hydrological processes, while the two-way nesting includes the vice versa. This implies, in two-way nesting, the outputs of the RCM models could be an input for the hydrological models and the output from the hydrological model can also be used to update the atmospheric models based on the feedback from the terrestrial models (Zabel & Mauser, 2013). Due to this fact, to improve the prediction skills of hydrometeorological models, the two-way coupling is generally superior over that of the one-way nesting (Kerandi et al., 2018). In areas where the soil moisture distribution is highly governed by the topography and its spatial and temporal correlation with the surface and lower atmosphere variables varies instantaneously, the coupled atmospheric-terrestrial model enables capable modelling system (Kerandi et al., 2018).

In Ethiopia, though there are emerging water resources developments (Berhanu et al., 2014), studies that combine the RCM with that of hydrological modelling for skilful hydrometeorological prediction few days to few months in advance are scarce. Therefore, this study is aiming at optimization of the WRF-Hydro model for hydrometeorological (mainly the Rainfall, Runoff and soil moisture) simulations at seasonal and sub-seasonal timescales. More specifically, this study will answer the following questions:

1. Can the WRF-hydro model reliably and accurately simulate the major hydrological components during the main rainy season (JJAS)?
2. Can the coupled WRF-Hydro model properly capture the extreme events of the hydrometeorological variables?
3. What are the sensitive WRF-Hydro parameters in simulating hydrometeorological variables in the Upper Tekeze basin?

4.3.1. Data

In-situ (satellite-based) observations such as daily rainfall observations (4.1.2.1), daily runoff observations and daily soil moisture observations and model forcing parameters such as the meteorological inputs and static geographic data for the time range of 2015-2020 will be used.

4.3.1.1. Discharge data

Daily runoff data for the period of 2015-2020 will be collected from the Ethiopian Ministry of Water Resources, Electricity and Irrigations (MWEI). These data are required for model calibration and verifications. The catchment has only one gauging station and is situated at the outlet. However, as the catchment size is more than 3500 square km with four sub-basins, an additional four new streamflow gauging stations will be constructed. The stations will be installed in four major stream channels in areas which might be ideal in measuring the required runoff and geologically stable for a long period of time, more preferably in bridges close to the outlet of each sub-basins. The stations will be monitored for a period of two years (2019-2020).

4.3.1.2. Soil moisture data

In this research work, together with streamflow, the soil moisture characteristics under different rainfall conditions will be simulated. However, for model verifications, soil moisture data is among the data drought fields in the study area. Hence, satellite-based soil moisture data (i.e., SM-DAS-2) will be retrieved from the H-SAF database (EUMETSAT server) at the website: http://hsaf.meteoam.it/soil-moisture.php. The SM-DAS-2 is the H-SAF root zone soil moisture index product based on Advanced Scatterometer (ASCAT) surface soil moisture data assimilation in the ECMWF Land Data Assimilation System. The database provides continuous estimates of soil moister at 4 layers: 0-7 cm, 7-28 cm, 28-100 cm, 100-289 cm below the surface, 25 km horizontal resolutions and 24-hour time step, with global daily coverage at 00:00 UTC. It is a global product of consistent surface and root zone soil moisture available near real-time for NWP, climate and hydrological communities. Nevertheless, this dataset shall be validated with in-situ observations. For this reason, representative moisture sensors will be established in convenient areas where meteorological compounds and schools are found in and around the catchment. In-situ soil moisture observations up to the root depth (~1.5 m deep) will be measured for two years (2019-2020).

4.3.1.3. Watershed characteristics: soil, water abstraction, land use and topography

Watershed information such as soil properties (soil depth and soil texture), daily average water abstraction for different purposes, the land uses and terrain characteristics in the entire catchment are also among the important factors that affect model verification, simulation and prediction. These parameters will be collected through field survey to be conducted within the Zamra catchment (study area) and also derived from secondary sources such as Bureau of Water Resources and Irrigation for water abstraction, preferably from the Regional Agricultural Bureau, under which administrative units of the watershed is situated. Land use and topography information will be obtained from the Ethiopian Mapping Agency (EMA) and others sources at high resolution (30m or higher) such as Shuttle Radar Topography Mission (SRTM) and Hydrological data and maps based on Shuttle Elevation Derivatives at multiple Scales (HydroSHEDS) from U.S. Geological Survey (USGS) and Sentinel (2) from European Space Agency (ESA). Representative ground control points (GCP) for land use classification validation will be gathered using GPS and by preparing transect walk maps and land use data record sheets.

4.3.1.4. Model input data

The model forcing terrestrial inputs and meteorological data such as incoming shortwave and longwave radiation (W/m^2), 2m-height specific humidity (kg/kg), 2m-height air temperature (K), surface

pressure(Pa), 10m-height surface wind in the horizontal and vertical component (m/s), liquid water precipitation rate(mm/s) will be extracted from WRF model (Kerandi et al., 2018). These data will be developed in a netCDF format to be reused by the WRF-Hydro model. For the routing modules, additional input fields such as maximum soil moisture, infiltration capacity excess, lateral surface hydraulic conductivity for each soil type and the soil moisture content for each soil layer will also be extracted from the Noah LSM. In addition to the aforementioned datasets, channel network data of the catchment will be acquired for accurately routing the hydrological process across the land surface. This input dataset will be prepared using the WRF-Hydro GIS Pre-Processing tool Version 5 (Sampson & Gochis, 2018).

4.3.2. WRF-Hydro model description and configurations

The coupled WRF-Hydro model is a, fully distributed, combination of the WRF model (see details in section 4.2 and Skamarock et al., 2008) and WRF-hydrological model which is an extended version of the WRF model for hydrological modelling system (Gochis et al., 2018). This modelling system is a modelling architecture that enhances coupling of multiple hydrological processes which includes the spatially distributed land surface models, sub-surface flow routing models, overland and channel flow routing, conceptual baseflow models with that of the atmospheric models (Figure 4.8). The current version of WRF-Hydro (version 5.0) is designed in a way that can facilitate improved representations of the terrestrial hydrological process at higher spatial resolution (i.e., 1 km or less) using a variety of physics-based and conceptual approaches. The WRF-Hydro model can also be operated in a standalone (in an "uncoupled/offline") manner as traditional land surface hydrological modelling system. Detailed information of the WRF-Hydro model is found in the WRF-Hydro modelling technical description (Gochis et al., 2018).

The WRF-Hydro modelling system requires several input files that describes the model domain, parameters and initial conditions (Figure 4.9). The coding of the WRF-hydro system is flexible to accommodate these different input variables depending on the domain configurations. This will be done either by calling from the WRF model and/or by running in a standalone mode. The demand for input variables also depends on the selection of the model physics options and sub-component routing functions (Figure 4.8). In this study, a two-way coupled WRF-Hydro model version 5.0 with Noah-MP LSM physical option will be used (Gochis et al., 2018). This will be executed by nesting the meteorological inputs and land surface model from the inner domain do3 (Figure 4.6a). This will be performed by combining the geogrid files and meteorological forecast from WRF model with that of the high-resolution hydrologically conditioning data (USGS HydroSHEDS: Lehner et al., 2006), using the WRF-Hydro GIS-Preprocessing tool Version 5 (Sampson & Gochis, 2018) and the Noah SLM aggregation/disaggregation process. The domain-d03 with 3 km horizontal resolution will be further disaggregated by a factor of 10 (Gochis et al., 2018) to form a high-resolution (300mX300m) hydrological routing grids-i.e., H300m (Figure 4.10b). The hydrological routing will be defined with a threshold of 80 contributing grid cells, that is from around 7.2 km^2 with routing timesteps of the 20 seconds. This routing grid resolution is within the finest terrain scale category that can be effective in formulating overland flow routings and in agreement with the recommendations of Gochis et al. (2018). Henceforth, all the hydrometeorological simulations will be based on the coupling processes between the atmospheric simulation on the domain-d03 and the routing processes on the 300m grid resolutions (Figure 4.10).

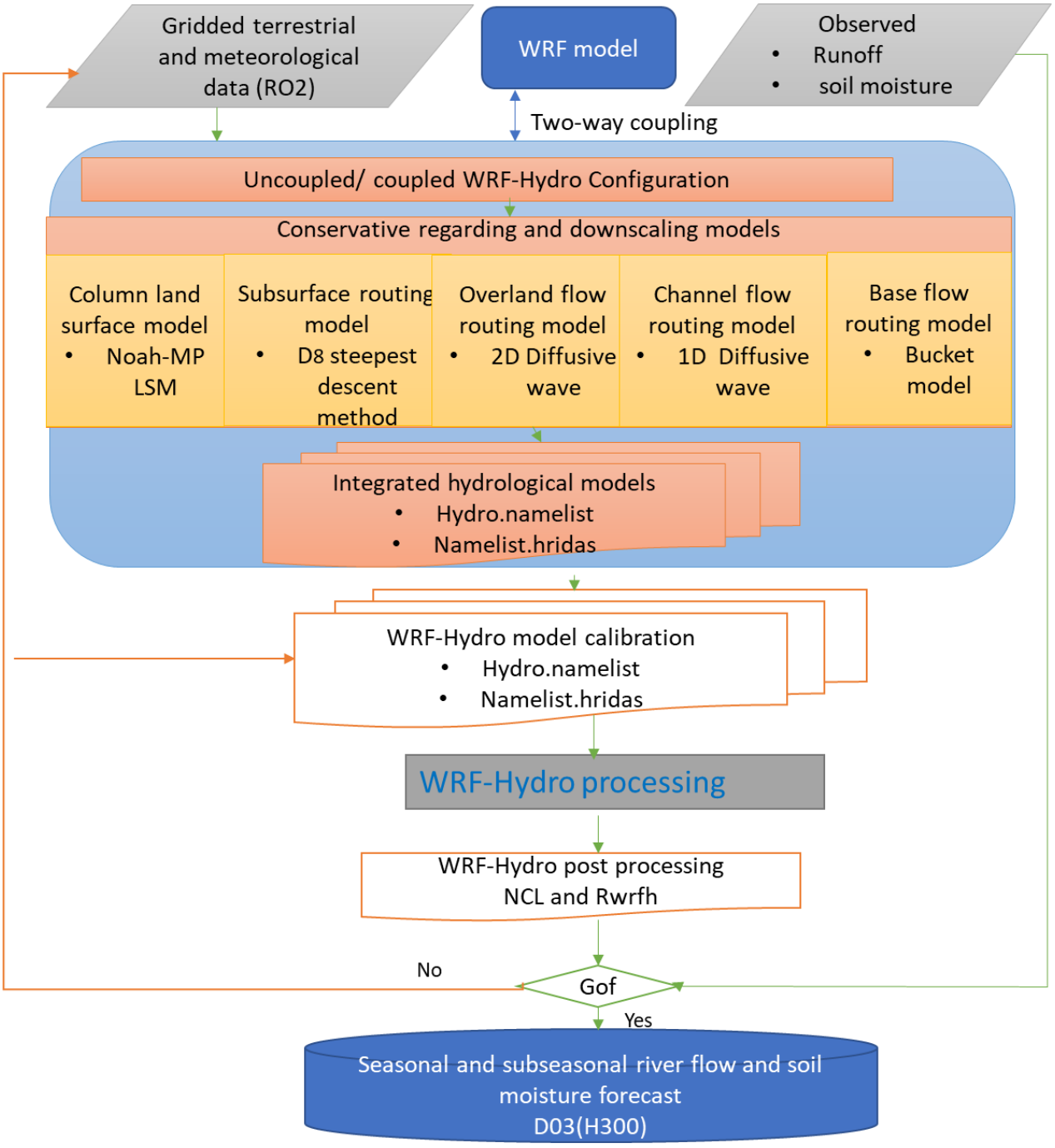

Figure 4.8. Generalized conceptual schematic WRF-Hydro architecture showing the various categories of model components (adapted from Gochis et al. (2018)).

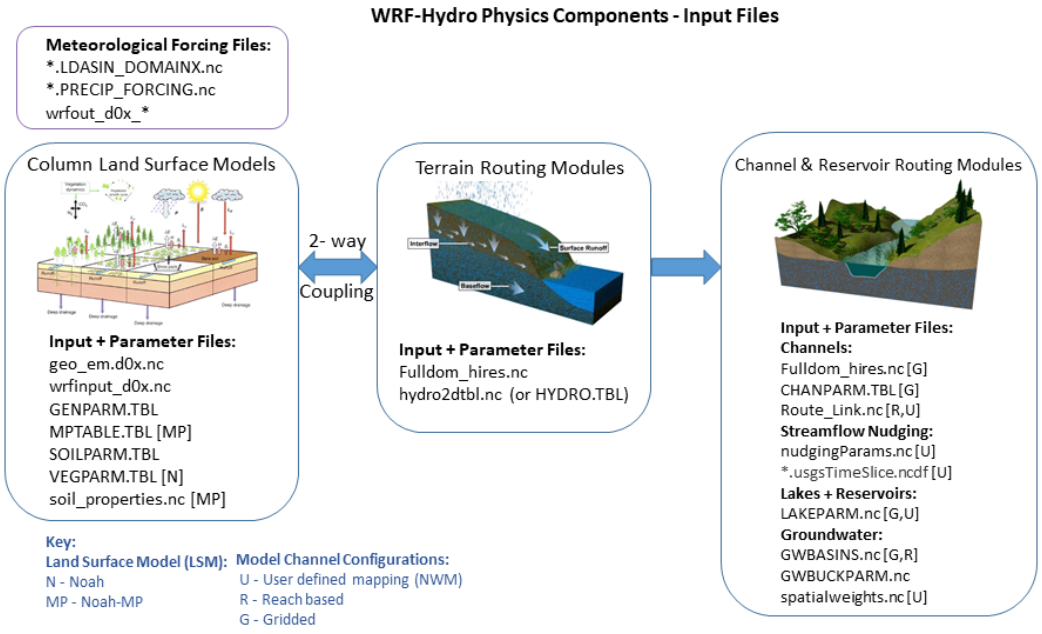

Figure 4.9: WRF-Hydro model configurations with input and parameter files organized by the model physics component (Gochis et al., 2018).

In order to attain reliable coupling of the WRF-Hydro modelling system, the model needs additional efforts of functional modifications in relation to domain interest. For the routing process, the physical options such as the surface overland flow, subsurface flow, channel routing and baseflow will be activated.

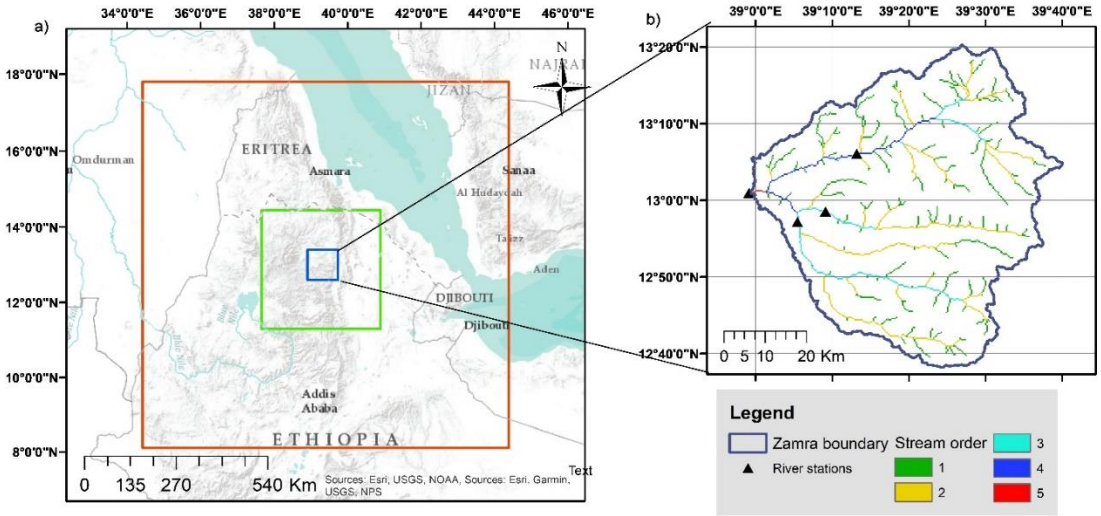

Figure 4.10: the study area together with the nested configurations of WRF domains at 27 km, 9km and 3km resolution in the red, green and blue boxes in (a) and WRF-Hydro configuration and channel networking at 300m resolution with 80 number of contributing grids, five stream orders and four river stations in (b).

4.3.2.1. Subsurface routing

The subsurface lateral flow will be estimated prior to the routing of overland flow (Gochis et al., 2018; Yucel et al., 2015). This is because exfiltration from fully saturated grid cells is added to the infiltration excess calculated from the LSM that ultimately update the surface head prior to routing of overland flow. In the WRF-Hydro default model implementations, a supersaturated soil column with 2-m soil depth is defined as a soil column that possesses a positive subsurface moisture flux. This saturated soil column is assumed to have four soil layers with a thickness of 10, 30, 60 and 100 cm from the top surface. Though the choice of soil layer configurations is quite subjective (Naabil et al., 2017), the model is flexible to manually specify the soil depths and respective thickness depending on the domain characteristics. For this study, assuming a soil depth of the root zone (~1.5 m) and in agreement with Naabil et al. (2017) and H-SAF for soil moisture monitoring, the subsurface routing model will be configured in four layers with a depth to the bottom layer of 7, 28, 100 and 200 cm from the surface. This is flexible to accommodate the in-situ soil column layer and their depth distribution from the field surveys.

The subsurface routing model with an eight-direction (D8) steepest descent method will be used to calculate the lateral flow of saturated soil moisture that represents a quasi-three-dimensional steady-state flow. The method includes the effects of topography, saturated soil depth, and saturated hydraulic conductivity. Using Dupuit-Forchheimer assumptions (Gochis et al., 2018), for a fixed grid cell size X_{ij}, (i^{th} column and j^{th} row), the saturated subsurface flow rate from X_{ij} cell (q_{ij}) at time *t* will be calculated as:

$$q_{ij} = T_{ij}\beta_{ij}W_{ij}\ when\ \beta_{ij} < 0 \ldots\ldots\ldots\ldots (Equ.2)$$

$$= 0 \quad when\ \beta_{ij} < 0$$

Where T_{ij} is the transmissivity of the cell, W_{ij} is the width of the cell, β_{ij} is the water table slope and is calculated as the difference in water table depths between two adjacent grid cells divided by the grid spacing.

4.3.2.2. Surface overland flow routing

In this study, for the overland flow calculation, a 2-dimensional, spatially explicit, fully-unsteady, finite-difference, diffusive wave algorithm will be used. The model accounts for backwater effects and allows for flow on adverse slopes (Naabil et al., 2017). Though it needs high computing resources, this method provides an accurate estimation of water movements across complex land surfaces (Gochis et al., 2018). The 2-dimensional diffusive wave equation uses the simplified version of the general Saint-Venant continuity equations as:

$$\frac{\partial h}{\partial t} = \frac{\partial q_x}{\partial x} + \frac{\partial q_y}{\partial x} = i_e \ldots\ldots\ldots\ldots\ldots\ldots (Equ.3)$$

where *h* is the surface flow depth; q_x and q_y are the unit discharges in the x- and y-directions, respectively; and i_e is the infiltration excess. In WRF-Hydro, the 2-dimensional flow across each terrain grid is calculated first in the x- then in the y-direction (Gochis et al., 2018). For instance, the overland flow in x- direction (q_x) will be estimated using the Manning's equation as:

$$q_x = \alpha_x h^{\beta} \ldots\ldots\ldots\ldots\ldots\ldots\ldots\ldots\ldots\ldots (Equ.4)$$

Where $\alpha_x = \frac{S_{fx}^{1/2}}{n_{ov}}$, n_{ov} is the roughness coefficient of the land surface and is a tunable parameter and β is a unit dependent coefficient expressed here as 5/3 for SI units and S_{fx} is the friction slope in the x-direction described as:

$$S_{fx} = S_{ox} - \frac{\partial h}{\partial x} \ldots\ldots\ldots\ldots\ldots\ldots\ldots\ldots (Equ. 5)$$

Where S_{ox} is the terrain slope in the x-direction and $\frac{\partial h}{\partial x}$ is the change in depth of the water surface above the land surface in the x-direction.

4.3.2.3. Channel and reservoir routing

For this study, the channel routing process with SLM gridded routing algorithms will be configured. The algorithm is based on a mass balance equation (a simplified version of the Saint-Venant continuity equation) for shallow water flow with one dimensional, variable time stepping diffusive wave formation (Gochis et al., 2018). This channel routing model will be defined in a pixel by pixel size (300mX300m) distributed across the predefined channel network of the domain. This is based on the principle that the water from each gridded cell transfers to the next cell in the channel network if the depth of ponded water (or surface head, 'SFCHEADRT') in each gridded cells exceeds a predefined retention depth ('RETDEPRT') (Gochis et al., 2018).

The flow from each pixel is the only upstream-to-downstream direction. Within every channel grid cell, the channel geometry will assume as a trapezoidal shape with channel parameters such as stream Strahler order (St order), bottom width (Bw), initial water depth (HLINK), channel side slope (Ch SSlp) and Manning's roughness coefficient (MannN). In the WRF-Hydro model, the default channel parameters are presented in Table 4.4. In this study, except Manning's coefficient, all channel geometric properties will be set to their default values. This is consistent with Kerandi et al. (2018) and Yucel et al. (2015) that in areas with no sufficient channel cross-section data, maintaining the default values is practical. The only parameter that needs calibrations because of its significant role in changing the river flow hydrograph is the MannN parameter (Silver et al., 2017; Yucel et al., 2015).

Table 4.4. Default channel parameter values (Kerandi et al., 2018; Naabil et al., 2017; Yucel et al., 2015)

St Order	Bw	HLINK	Ch SSlp	MannN
1	5	0.02	3	0.65
2	10	0.02	1	0.5
3	20	0.02	0.5	0.45
4	30	0.03	0.18	0.35
5	40	0.03	0.05	0.20
6	60	0.03	0.05	0.12
7	60	0.03	0.05	0.03

Having these input data, the streamflow in an open channel (Q in m^3/s) will be estimated as function of flow hydraulics, channel storage and the lateral inflow contribution from each grid cell using the diffusive wave approximation (i.e., by ignoring the convective term in the momentum equation (Gochis et al., 2018; Yucel et al., 2015)) as :

$$Q = -SIGN\left(\frac{\partial Z}{\partial x}\right) K \sqrt{\left|\frac{\partial Z}{\partial x}\right|} \ldots\ldots\ldots\ldots\ldots\ldots\ldots\ldots\ldots\ldots (Equ.6)$$

Where the $\frac{\partial Z}{\partial x}$ is the fractional slope, the *SIGN* function is 1 for $\frac{\partial Z}{\partial x}$ >0 and -1 for $\frac{\partial Z}{\partial x} < 0$, *Z* water surface elevation (m), and *K* is from the Manning's equation (m^3/s) computed conveyance given by:

$$K = \frac{Cm}{n} A\, R^{2/3} \ldots\ldots\ldots\ldots\ldots\ldots\ldots\ldots\ldots\ldots (Equ.7)$$

Where *n* is Manning's roughness coefficient, A is the cross-sectional area (m^2), *R* hydraulic radius (m) and *Cm* is the dimensional constant (1.0 for SI units).

4.3.2.4. Conceptual baseflow process

In WRF-Hydro streamflow simulation, the baseflow parameter will be activated to conceptually (i.e. not physically-explicit) account the contributions of baseflow to streamflow. Herein, the groundwater flow system to stream network will be represented using a simple, empirical "catchment storage-discharge bucket model" with conceptual depth and storage capacity (Gochis et al., 2018; Senatore et al., 2015). In areas with lack of specific regional groundwater process information like Zamra catchment, the baseflow basin in WRF-Hydro is assumed to be the same as the topographic surface and the buckets can be defined from a true aquifer or hydrographic dataset such as, in this case, the USGS HydroSHEDS (Sampson & Gochis, 2018). For gridded channel routing, the total basin baseflow flux to the stream network is assumed to be equally distributed among all channel pixels within a catchment. Nevertheless, it is important to notice that this bucket model is highly abstracted and conceptualized representation of groundwater processes in that the depth of water values in the bucket and the parameters themselves do not refer to the actual aquifer systems (Gochis et al., 2018). Thus, the baseflow as part of streamflow will be estimated based on an exponential storage-discharge function as a function of a conceptual depth of water in the bucket "i'' as:

$$Q_{bucket\ out,i} = Coeff_i\, e^{Expon_i} \frac{Z_i}{Zmax_i}\ where\ Z_i \leq\ Zmax_i$$

$$= \mathrm{Q}_{\mathrm{bucket\ in,i,}}\quad where\ Z_i > Zmax_i \ldots\ldots\ldots\ldots (Equ.8)$$

Where $\mathrm{Q}_{\mathrm{bucket\ out}}$ is the outflow from the bucket model as baseflow, $\mathrm{Q}_{\mathrm{bucket\ in}}$ is the bucket model inflow as recharge, *Coeff* is the bucket model coefficient, *Expon* is the bucket model exponent, Z is the initial depth of water in the bucket model, and $Zmax$ is the maximum storage in the bucket before draining occurs. The initial values of the groundwater bucket model parameters are initially estimated analytically or 'offline' from WRF-Hydro and then can be modified through model calibration. The overall streamflow of the catchment will be then estimated by combining the baseflow from the bucket model with that of the lateral inflow from the overland flow that directly joins to the stream network.

4.3.3. Model calibration

The WRF-Hydro modelling system uses several parameters associated with ocean-atmosphere-terrestrial factors. Thus, the use of the WRF-Hydro model for hydrometeorological simulations needs proper calibration. For this study, a "step-wise'' manual calibration procedure that controls the volume of hydrological variables and then their temporal variation will be executed. This ensures that a model that

potentially simulate the volume of the hydrological components can later be calibrated in response to the time variations. In such calibration techniques and models with multi-parameters, parameters interaction effect is expected (Silver et al., 2017; Yucel et al., 2015). Nevertheless, Yucel et al. (2015) have emphasized that theses interaction effects can be reduced by employing various performance measures (section 4.3.4). This has been further confirmed by Naabil et al. (2017) and Kerandi et al. (2018) in that calibration of the WRF-Hydro model manually with a step-wise approach have shown improved skills.

Herein, the response of coupled WRF-Hydro in simulating the runoff and soil moisture to the weights of four major factors: (1) the surface runoff parameter i.e., the infiltration scaling parameter (REFKDT), (2) surface retention depth scaling parameter (RETDEPRT), (3) overland flow roughness scaling parameter (OVROUGHRTFAC), (4) the channel Manning roughness coefficient scaling parameter (MannN) will be assessed. As a control simulation, the WRF-Hydro model will be running by maintaining the parameters at their default value. Next, the REFKDT and RETDEPRT parameters will be calibrated controlling the volume of the runoff and soil moisture content. The values of REFKDT and RETDEPRT varies in a range 0.1-10 and 0.0-5.0, While the model default values are 3.0 and 1.0, respectively. In the last step, the response of the river hydrograph shape and soil moisture graph in relation to different values of OVROUGHRTFAC (0.0-1.0) and MannN will be calibrated. The OVROUGHRTFAC parameter is an important parameter of the Noah LSM model which decides the amount of excess water that can transfer to the channel network. The shape of the hydrograph can also be affected by the channel properties of the river geometry (Table 4.3). The default values of channel Manning's roughness coefficients presented in Table 4.3 are based on textbook values (Yucel et al., 2015). For every run in the calibration of the WRF-Hydro model in response to the change of MannN value, instead of changing Manning coefficient for different stream order individually, the use of scale factor is a more practical approach (Kerandi et al., 2018; Yucel et al., 2015). Herein, the scale factor which ranges from 0.6 to 2.1 with 0.1 increments will be employed as a calibration parameter of the MannN.

For this calibration, in agreement with recent studies (Kerandi et al., 2018; Silver et al., 2017; Yucel et al., 2015), the uncoupled WRF-Hydro modelling will be used. Herein, the forcing initials such as the meteorological and geographical inputs will be remapped from the WRF model and a gridded netCDF format files will be prepared (Gochis et al., 2018). The optimal parameter values will be then selected by comparing simulated values with that of the in-situ hydrometeorological observations. For the calibrations, one/two year of discharge data (2019 or/and 2020) and for validation 2021 will be used. These time series are selected considering the availability of observed dat. The use of one-two years' time series data in WRF-Hydro model verification is a common practice (Naabil et al., 2017; Silver et al., 2017) and reasonably enough (Kerandi et al., 2018).

4.3.4. Performance evaluation

The performance of the WRF-Hydro model in simulating the hydrometeorological variables will be assessed using four error statistical methods (Appendix: section 8.1): the Nash-Sutcliffe Efficiency (NSE) given by $Equ.8.9$ and the RMSE ($Equ.8.5$), ME ($Equ.8.2$) and Pearson correlation coefficient ($Equ.8.1$). This will be supported by the Taylor diagrams (Taylor, 2001) which will be employed to visualize the strength and weakens of different WRF-Hydro calibrations and configurations in reproducing the observed runoff and soil moisture values.

4.4. Summary of a proposed methodological framework

Generally, the schematic workflow and the overall methods are presented in Figure 4.11.

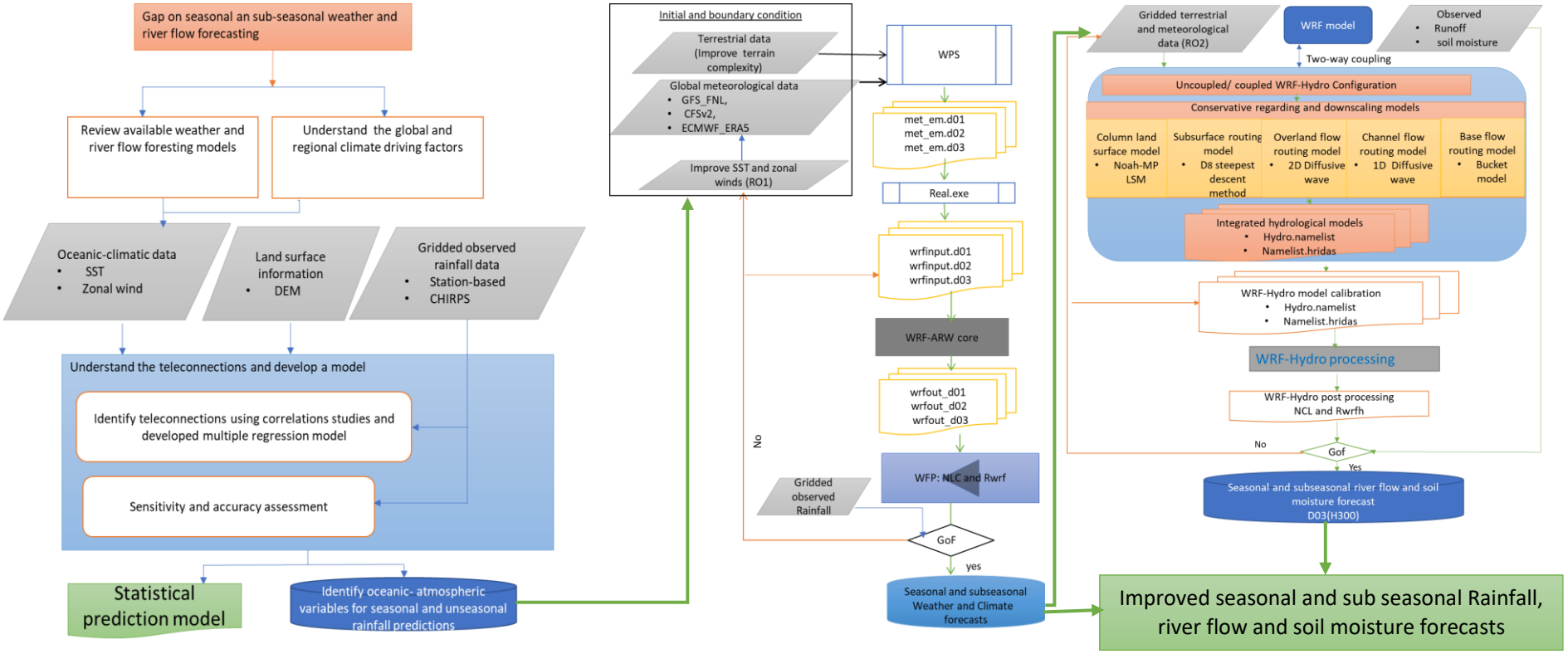

Figure 4.11: Summarized schematic workflow to improve seasonal and sub-seasonal rainfall, river flow and soil moisture predictions over Northern Ethiopia.

5. Expected output

At the end of this project work, the following research outputs are expected

- A review of existing seasonal and sub-seasonal prediction methods;
- A JJAS rainfall prediction framework based on oceanic-atmospheric teleconnections
- Customized numerical weather and climate prediction model for seasonal and sub-seasonal prediction over Northern Ethiopia;
- JJAS rainfall distribution maps at 3km or less spatial resolution and daily, monthly, sub-seasonal and seasonal timescales for Northern Ethiopia;
- Joint atmospheric-terrestrial model for seasonal and sub-seasonal hydrometeorological and streamflow predictions
- Three (four) paper in high impact peer-reviewed journals;
    - Investigate the teleconnections between global climate driving factors and seasonal and sub-seasonal rainfall variation over Northern Ethiopia
    - Customize the WRF model as a regional climate model for seasonal and sub-seasonal rainfall prediction in Northern Ethiopia
    - Sensitivity analysis of global SST and zonal winds in a complex topography in the prediction of the JJAS rainfall at seasonal and sub-seasonal timescales over northern Ethiopia.
    - Joint atmospheric-terrestrial (WRF-Hydro) modelling for seasonal and sub-seasonal hydrometeorological predictions in Upper Tekeze Basin, Northern Ethiopia.
- Two MSc thesis:
    - over Northern Ethiopia: a case study of
        - Spatio-temporal precipitation trend analysis
        - Water abstraction for agricultural production
- One dissertation: seasonal and sub-seasonal rainfall and river flow prediction over Northern Ethiopia
- Policy brief documents from the major research findings for proper planning land use dynamics, early warning, preparedness, disaster protection.

6. Research and academic work plan

Table 6.1: the time frame for the overall PhD project work. Where Q represents a length of three months of a year. In the Table hereunder, as the PhD is a sandwich program, the overall time distribution between ITC, UT and Mekelle University (MU), Ethiopia are also indicated in yellow and blue shades, respectively. As per the schedule, some data such as forcing initials (meteorological and static data) from NCAR, Research Data Archive (website: https://rda.ucar.edu/); oceanic- atmospheric data (SST and Zonal wind, climate indices data) and CHIRPS data from IRI, Climate Data Library(website: http://iridl.ldeo.columbia.edu/) and observed daily rainfall data from NMA, Ethiopia were collected.

No	Activity	Years															
		I (July 2018- June 2019)				II (July 2019- June 2020)				III (July 2020- June 2021)				IV (July 2021- June 2022)			
		ITC, UT			MU, Ethiopia				ITC, UT	MU, Ethiopia				ITC, UT			
		Q1	Q2	Q3	Q4	Q1	Q2	Q3	Q4	Q1	Q2	Q3	Q4	Q1	Q2	Q3	Q4
1	Literature review																
2	Proposal development																
3	Coursework and Training																
4	Qualifier																
5	Year I. Progress Report																
6	Fieldwork 1: data collection for Objective 1 and 2																
7	Data analysis and paper write up of for objectives 1 and 2 and submission paper 1 and 2 for publication																
8	Seminar participation																
9	Year II. Progress Report																
7	Fieldwork 2: data collection for Objective 3																
8	Data analysis and paper write up for Objective 3 and 4 and submission 3rd paper for publication																
9	Year III. Progress Report																
10	Fourth paper write up and submission for publication																
11	Incorporate comments and suggestions																
12	Final thesis organization, synthesis, and submission																
13	Defence																

7. References

Abdelwares, M., Haggag, M., Wagdy, A., & Lelieveld, J. (2017). Customized framework of the WRF model for regional climate simulation over the Eastern NILE basin. *Theoretical and Applied Climatology*, 1–17. https://doi.org/10.1007/s00704-017-2331-2

Aggarwal, R. (2013). A Comprehensive Review of Numerical Weather Prediction Models. *International Journal of Computer Applications*, *74*(18), 44–48.

Amir Erfanian, Guiling Wang, Miao Yu1, R. A., Sikder, S., & Faisal, H. (2016). Journal of Advances in Modeling Earth Systems. *Journal of Advances in Modeling Earth Systems*, (13 SEP 2016), 1411–1431. https://doi.org/10.1002/2016MS000660.Received

Andrys, J., Lyons, T. J., & Kala, J. (2015). Multidecadal evaluation of WRF downscaling capabilities over Western Australia in simulating rainfall and temperature extremes. *Journal of Applied Meteorology and Climatology*, *54*(2), 370–394. https://doi.org/10.1175/JAMC-D-14-0212.1

Argent, R., Sun, X., Semazzi, F., Xie, L., & Liu, B. (2015). The development of a customization framework for the WRF model over the Lake Victoria basin, eastern Africa on seasonal timescales. *Advances in Meteorology*, *2015*. https://doi.org/10.1155/2015/653473

Berhanu, B., Seleshi, Y., & Melesse, A. M. (2014). Surface Water and Groundwater Resources of Ethiopia: Potentials and Challenges of Water Resources Development. In *Nile River Basin* (pp. 97–117). Cham: Springer International Publishing. https://doi.org/10.1007/978-3-319-02720-3_6

Booji, M. J., van den Tillaart, S. P. M., & Krol, M. S. (2011). Risks in hydrological modelling due to uncertainties in discharge determination. *Risk in Water Resources Management*, (July), 95–100.

Borovikov, A., Cullather, R., Kovach, R., Marshak, J., Vernieres, G., Vikhliaev, Y., … Li, Z. (2017). GEOS-5 seasonal forecast system. *Climate Dynamics*, *0*(0), 1–27. https://doi.org/10.1007/s00382-017-3835-2

Bourgin, F., Ramos, M. H., Thirel, G., & Andréassian, V. (2014). Investigating the interactions between data assimilation and post-processing in hydrological ensemble forecasting. *Journal of Hydrology*, *519*(PD), 2775–2784. https://doi.org/10.1016/j.jhydrol.2014.07.054

Brown, J. D., Demargne, J., Seo, D. J., & Liu, Y. (2010). The Ensemble Verification System (EVS): A software tool for verifying ensemble forecasts of hydrometeorological and hydrologic variables at discrete locations. *Environmental Modelling and Software*, *25*(7), 854–872. https://doi.org/10.1016/j.envsoft.2010.01.009

Brown, J. N., Hochman, Z., Holzworth, D., & Horan, H. (2018). Seasonal climate forecasts provide more definitive and accurate crop yield predictions. *Agricultural and Forest Meteorology*, *260–261*(February), 247–254. https://doi.org/10.1016/j.agrformet.2018.06.001

Buizza, R. (2018). *Chapter 2 – Ensemble Forecasting and the Need for Calibration*. *Statistical Postprocessing of Ensemble Forecasts*. Elsevier Inc. https://doi.org/10.1016/B978-0-12-812372-0.00002-9

Camberlin, P. (1997). Rainfall anomalies in the source region of the Nile and their connection with the Indian summer monsoon. *Journal of Climate*, *10*(6), 1380–1392. https://doi.org/10.1175/1520-0442(1997)010<1380:RAITSR>2.0.CO;2

Camberlin, P., Janicot, S., & Poccard, I. (2001). Seasonality and atmospheric dynamics of the teleconnection between African rainfall and tropical sea-surface temperature: Atlantic vs.

ENSO. *International Journal of Climatology*, *21*(8), 973–1005. https://doi.org/10.1002/joc.673

Camberlin, P., & Philippon, N. (2002). The East African March-May Rainy Season : Associated Atmospheric Dynamics and Predictability over the 1968 – 97 Period. *Journal of Climate*, *15*(9), 1002–1019. https://doi.org/http://dx.doi.org/10.1175/1520-0442(2002)015%3C1002:TEAMMR%3E2.0.CO;2

Carvalho, D., Rocha, A., Gómez-Gesteira, M., & Santos, C. (2012). A sensitivity study of the WRF model in wind simulation for an area of high wind energy. *Environmental Modelling & Software*, *33*, 23–34. https://doi.org/10.1016/J.ENVSOFT.2012.01.019

Chen, C. J., & Georgakakos, A. P. (2015). Seasonal prediction of East African rainfall. *International Journal of Climatology*. https://doi.org/10.1002/joc.4165

Degefu, M. A., Rowell, D. P., & Bewket, W. (2017). Teleconnections between Ethiopian rainfall variability and global SSTs: observations and methods for model evaluation. *Meteorology and Atmospheric Physics*, *129*(2), 173–186. https://doi.org/10.1007/s00703-016-0466-9

Dinku, T., Funk, C., Peterson, P., Maidment, R., Tadesse, T., Gadain, H., & Ceccato, P. (2018). Validation of the CHIRPS satellite rainfall estimates over eastern Africa. *Quarterly Journal of the Royal Meteorological Society*. https://doi.org/10.1002/qj.3244

Diro, G. T., Grimes, D., Black, E., Parker, D. J., Priest, S. J., & Tapsell, S. M. (2008). Seasonal forecasting of Ethiopian spring rains. *Meteorological Applications*, *15*(January), 73–84. https://doi.org/10.1002/met.63

Diro, G. T., Grimes, D. I. F., & Black, E. (2011a). Teleconnections between Ethiopian summer rainfall and sea surface temperature: part I—observation and modelling. *Climate Dynamics*, *37*(1–2), 103–119. https://doi.org/10.1007/s00382-010-0837-8

Diro, G. T., Grimes, D. I. F., & Black, E. (2011b). Teleconnections between Ethiopian summer rainfall and sea surface temperature: Part II. Seasonal forecasting. *Climate Dynamics*, *37*(1), 121–131. https://doi.org/10.1007/s00382-010-0896-x

Diro, G. T., Tompkins, A. M., & Bi, X. (2012). Dynamical downscaling of ECMWF Ensemble seasonal forecasts over East Africa with RegCM3. *Journal of Geophysical Research Atmospheres*, *117*(16), 1–20. https://doi.org/10.1029/2011JD016997

Djibo, A., Karambiri, H., Seidou, O., Sittichok, K., Philippon, N., Paturel, J., & Saley, H. (2015). Linear and Non-Linear Approaches for Statistical Seasonal Rainfall Forecast in the Sirba Watershed Region (SAHEL). *Climate*, *3*(3), 727–752. https://doi.org/10.3390/cli3030727

ECMWF. (2017). ERA5 Reanalysis. Research Data Archive at the National Center for Atmospheric Research, Computational and Information Systems Laboratory. https://doi.org/https://doi.org/10.5065/D6X34W69.

EENSAT. (2018). EENSAT project. Retrieved September 12, 2018, from https://www.eensat.org/about-eensat/#background

Elsanabary, M. H., & Gan, T. Y. (2012). Investigation of seasonal rainfall variability over the Ethiopian Highlands: Teleconnection between the Upper Blue Nile Basin Rainfall and the Oceanic Anomalies. *Proceedings, Annual Conference - Canadian Society for Civil Engineering*, *1*(April 2014), 148–157. https://doi.org/10.13140/2.1.2164.0644

ENPC. (2016). *Federal Democratic Republic of Ethiopia: Groth and Transformation Plan II (GTP II).* (Vol. I).

Enyew, B.D., & Steeneveld, G. J. (2014). Analysing the Impact of Topography on Precipitation and

Flooding on the Ethiopian Highlands. *Journal of Geology & Geosciences*, *03*(06), 1–6. https://doi.org/10.4172/2329-6755.1000173

Fekadu, K. (2015). Ethiopian Seasonal Rainfall Variability and Prediction Using Canonical Correlation Analysis (CCA). *Earth Sciences*, *4*(3), 112. https://doi.org/10.11648/j.earth.20150403.14

Flaounas, E., Janicot, S., Bastin, S., & Roca, R. (2012). The West African monsoon onset in 2006: sensitivity to surface albedo, orography, SST and synoptic scale dry-air intrusions using WRF. *Climate Dynamics*, *38*(3–4), 685–708. https://doi.org/10.1007/s00382-011-1255-2

Force, A., Agency, W., Air, O., Base, F., Springs, C., Force, A., … Base, F. (2009). Weather Forecasts by the WRF-ARW Model with the GSI Data Assimilation System in the Complex Terrain Areas of Southwest Asia, 987–1008. https://doi.org/10.1175/2009WAF2222229.1

Frédéric, V., Andrew, W. R., & David, L. T. A. (2012). Subseasonal to Seasonal Prediction Project: bridging the gap between weather and climate. *WMO Bulletin 61 (2)*. Retrieved from http://www.wmo.int/pages/prog/arep/wwrp/new/documents/

Funk, C., Harrison, L., Shukla, S., Korecha, D., Magadzire, T., Husak, G., … Hoell, A. (2016). Assessing the Contributions of Local and East Pacific Warming to the 2015 Droughts in Ethiopia and Southern Africa. *Bulletin of the American Meteorological Society*, *97*(12), S75–S80. https://doi.org/10.1175/BAMS-D-16-0167.1

Funk, C., Hoell, A., Shukla, S., Bladé, I., Liebmann, B., Roberts, J. B., … Husak, G. (2014). Predicting East African spring droughts using Pacific and Indian Ocean sea surface temperature indices. *Hydrol. Earth Syst. Sci*, *18*, 4965–4978. https://doi.org/10.5194/hess-18-4965-2014

Funk, C., Peterson, P., Landsfeld, M., Pedreros, D., Verdin, J., Shukla, S., … Michaelsen, J. (2015). The climate hazards infrared precipitation with stations--a new environmental record for monitoring extremes. *Scientific Data*, *2*, 150066. https://doi.org/10.1038/sdata.2015.66

García-Díez, M., Fernández, J., Fita, L., & Yagüe, C. (2013). Seasonal dependence of WRF model biases and sensitivity to PBL schemes over Europe. *Quarterly Journal of the Royal Meteorological Society*, *139*(671), 501–514. https://doi.org/10.1002/qj.1976

Gebrechorkos, S. H., Hülsmann, S., & Bernhofer, C. (2018). Evaluation of multiple climate data sources for managing environmental resources in East Africa. *Hydrol. Earth Syst. Sci*, *22*, 4547–4564. https://doi.org/10.5194/hess-22-4547-2018

Gebrehiwot, T., van der Veen, A., & Maathuis, B. (2011). Spatial and temporal assessment of drought in the Northern Highlands of Ethiopia. *International Journal of Applied Earth Observation and Geoinformation*, *13*(3), 309–321. https://doi.org/10.1016/j.jag.2010.12.002

GFS. (2018). Global Forecast System (GFS) | National Centers for Environmental Information (NCEI) formerly known as National Climatic Data Center (NCDC). Retrieved September 8, 2018, from https://www.ncdc.noaa.gov/data-access/model-data/model-datasets/global-forcast-system-gfs

Girma, A., de Bie, C. A. J. M., Skidmore, A. K., Venus, V., & Bongers, F. (2016). Hyper-temporal SPOT-NDVI dataset parameterization captures species distributions. *International Journal of Geographical Information Science*, *30*(1), 89–107. https://doi.org/10.1080/13658816.2015.1082565

Gissila, T., Black, E., Grimes, D. I. F., & Slingo, J. M. (2004). Seasonal forecasting of the Ethiopian summer rains. *International Journal of Climatology*, *24*(11), 1345–1358. https://doi.org/10.1002/joc.1078

Givati, A., Lynn, B., Liu, Y., & Rimmer, A. (2012). Using the WRF model in an Operational Streamflow Forecast System for the Jordan River. *Journal of Applied Meteorology and Climatology*, *51*(2), 285–299. https://doi.org/10.1175/JAMC-D-11-082.1

Gleixner, S., Keenlyside, N., & Viste, E. (2017). Seasonal predictability of Ethiopian summer rainfall in climate models, *19*, 10422.

Gleixner, S., Keenlyside, N., Viste, E., & Korecha, D. (2017). The El Niño effect on Ethiopian summer rainfall. *Climate Dynamics*, *49*, 1865–1883. https://doi.org/10.1007/s00382-016-3421-z

Gobena, A. K., & Gan, T. Y. (2010). Incorporation of seasonal climate forecasts in the ensemble streamflow prediction system. *Journal of Hydrology*, *385*(1–4), 336–352. https://doi.org/10.1016/j.jhydrol.2010.03.002

Gochis, D. J., Barlage, M., Dugger, A., FitzGerald, K., Karsten, L., McAllister, M., … Yu, W. (2018). *The WRF-Hydro modelling system technical description, (Version 5.0)*. Retrieved from https://ral.ucar.edu/sites/default/files/public/WRF-HydroV5TechnicalDescription.pdf

Guo, Y., Li, J., & Li, Y. (2014). Seasonal forecasting of north China summer rainfall using a statistical downscaling model. *Journal of Applied Meteorology and Climatology*, *53*(7), 1739–1749. https://doi.org/10.1175/JAMC-D-13-0207.1

Harrison, M., Troccoli, A., Coughlan, M., & Williams, J. B. (2008). *Seasonal Forecasts in Decision Making*. *Seasonal Climate: Forecasting and Managing Risk* (Vol. 82). https://doi.org/10.1007/978-1-4020-6992-5

Hoedjes, J., Kooiman, A., Maathuis, B., Said, M., Becht, R., Limo, A., … Su, B. (2014). A Conceptual Flash Flood Early Warning System for Africa, Based on Terrestrial Microwave Links and Flash Flood Guidance. *ISPRS International Journal of Geo-Information*, *3*(2), 584–598. https://doi.org/10.3390/ijgi3020584

Hong, S.-Y., Leetmaa, A., Hong, S.-Y., & Leetmaa, A. (1999). An Evaluation of the NCEP RSM for Regional Climate Modeling. *Journal of Climate*, *12*(2), 592–609. https://doi.org/10.1175/1520-0442(1999)012<0592:AEOTNR>2.0.CO;2

Hoogenboom, G., Fraisse, C. W., Jones, J. W., Ingram, K. T., O'Brien, J. J., Bellow, J. G., … Roncoli, C. (2007). *Climate Prediction and Agriculture*. *Climate Prediction and Agriculture: Advances and Challenges*. https://doi.org/10.1007/978-3-540-44650-7

Huang, D., & Gao, S. (2017). Impact of different cumulus convective parameterization schemes on the simulation of precipitation over China. *Tellus A: Dynamic Meteorology and Oceanography*, *69*(1), 1406264. https://doi.org/10.1080/16000870.2017.1406264

Iguchi, T., Tao, W.-K., Wu, D., Peters-Lidard, C., Santanello, J. A., Kemp, E., … Loikith, P. (2017). Sensitivity of CONUS Summer Rainfall to the Selection of Cumulus Parameterization Schemes in NU-WRF Seasonal Simulations. *Journal of Hydrometeorology*, *18*(6), 1689–1706. https://doi.org/10.1175/JHM-D-16-0120.1

Jee, J., & Kim, S. (2017). Sensitivity Study on High-Resolution WRF Precipitation Forecast for a Heavy Rainfall Event. https://doi.org/10.3390/atmos8060096

Jung, S.-H., Im, E.-S., & Han, S.-O. (2012). The Effect of Topography and Sea Surface Temperature on Heavy Snowfall in the Yeongdong Region: A Case Study with High Resolution WRF Simulation. *Asia-Pacific J. Atmos. Sci*, *48*(3), 259–273. https://doi.org/10.1007/s13143-012-0026-2

Kerandi, N., Arnault, J., Laux, P., Wagner, S., Kitheka, J., & Kunstmann, H. (2018). Joint atmospheric-terrestrial water balances for East Africa: a WRF-Hydro case study for the upper Tana River

basin. *Theoretical and Applied Climatology*, *131*(3–4), 1337–1355. https://doi.org/10.1007/s00704-017-2050-8

Kerandi, N. M., Laux, P., Arnault, J., & Kunstmann, H. (2017). Performance of the WRF model to simulate the seasonal and interannual variability of hydrometeorological variables in East Africa: a case study for the Tana River basin in Kenya. *Theoretical and Applied Climatology*, *130*(1–2), 401–418. https://doi.org/10.1007/s00704-016-1890-y

Kirtman, B. P., Min, D., Infanti, J. M., Kinter, J. L., Paolino, D. A., Zhang, Q., … Wood, E. F. (2014). The North American Multimodel Ensemble: Phase-1 Seasonal-to-Interannual Prediction; Phase-2 toward Developing Intraseasonal Prediction. *Bulletin of the American Meteorological Society*, *95*(4), 585–601. https://doi.org/10.1175/BAMS-D-12-00050.1

Klemm, T., & McPherson, R. A. (2017). The development of seasonal climate forecasting for agricultural producers. *Agricultural and Forest Meteorology*, *232*, 384–399. https://doi.org/10.1016/j.agrformet.2016.09.005

Korecha, D., & Barnston, A. G. (2007). Predictability of June–September Rainfall in Ethiopia. *Monthly Weather Review*, *135*(2), 628–650. https://doi.org/10.1175/MWR3304.1

Korecha, D., & Sorteberg, A. (2013). Validation of operational seasonal rainfall forecast in Ethiopia. *Water Resources Research*, *49*(11), 7681–7697. https://doi.org/10.1002/2013WR013760

Kumar, A., Zhang, L., Wang, W., Kumar, A., Zhang, L., & Wang, W. (2013). Sea Surface Temperature–Precipitation Relationship in Different Reanalyses. *Monthly Weather Review*, *141*(3), 1118–1123. https://doi.org/10.1175/MWR-D-12-00214.1

Kusunose, Y., & Mahmood, R. (2016). Imperfect forecasts and decision making in agriculture. *Agricultural Systems*, *146*, 103–110. https://doi.org/10.1016/j.agsy.2016.04.006

Lakew, D., Carucci, V., Wendem-Ageňehu, A., & Abebe, Y. (2005). Community-based participatory watershed development : A Guideline Annex Community-based Participatory Watershed Development : *A Guideline.Ministry of Agriculture and Rural Development, Addis Ababa, Ethiopia.*

Lehner, B., Verdin, K., & Jarvis, A. (2006). *HydroSHEDS Technical Documentation Version 1.0*. Retrieved from http://hydrosheds.cr.usgs.gov

Li, L., Li, W., & Jin, J. (2014). Improvements in WRF simulation skills of southeastern United States summer rainfall: physical parameterization and horizontal resolution. *Climate Dynamics*, *43*(7–8), 2077–2091. https://doi.org/10.1007/s00382-013-2031-2

Lin, P., Yang, Z. L., Gochis, D. J., Yu, W., Maidment, D. R., Somos-Valenzuela, M. A., & David, C. H. (2018). Implementation of a vector-based river network routing scheme in the community WRF-Hydro modelling framework for flood discharge simulation. *Environmental Modelling and Software*, *107*(May), 1–11. https://doi.org/10.1016/j.envsoft.2018.05.018

Lu, D., White, L., Reddy, R. S., Williams, Q. L., & Croft, P. J. (2011). Multiseason evaluation of the MM5, COAMPS and WRF over southeast United States. *Meteorology and Atmospheric Physics*, *111*(3–4), 75–90. https://doi.org/10.1007/s00703-011-0124-1

MacLachlan, C., Arribas, A., Peterson, K. A., Maidens, A., Fereday, D., Scaife, A. A., … Madec, G. (2015). Global Seasonal forecast system version 5 (GloSea5): a high-resolution seasonal forecast system. *Quarterly Journal of the Royal Meteorological Society*, *141*(689), 1072–1084. https://doi.org/10.1002/qj.2396

McIntosh, P. C., Pook, M. J., Risbey, J. S., Lisson, S. N., & Rebbeck, M. (2007). Seasonal climate

forecasts for agriculture: Towards better understanding and value. *Field Crops Research*, *104*(1–3), 130–138. https://doi.org/10.1016/j.fcr.2007.03.019

Murphy, S., Washington, R., Downing, T., Martin, R., Ziervogel, G., Todd, A. P. M., … Briden, J. (2001). Seasonal forecasting for climate hazards: prospect and responses. *Natural Hazards*, *23*, 171–196.

Naabil, E., Lamptey, B. L., Arnault, J., Kunstmann, H., & Olufayo, A. (2017). Water resources management using the WRF-Hydro modelling system: Case-study of the Tono dam in West Africa. *Journal of Hydrology: Regional Studies*, *12*(May), 196–209. https://doi.org/10.1016/j.ejrh.2017.05.010

NASEM. (2016). *Next Generation Earth System Prediction: Strategies for Subseasonal to Seasonal Forecasts*. *The National Academies Press* (Vol. 4). Washington, D.C.: The National Academies Press. https://doi.org/10.17226/21873

NCAR. (2018). NCAR Research Data Archive (NCAR RDA). Retrieved October 18, 2018, from http://www2.mmm.ucar.edu/wrf/users/download/free_data.html

NCEP. (2015). NCEP GDAS/FNL 0.25 Degree Global Tropospheric Analyses and Forecast Grids. Research Data Archive at the National Center for Atmospheric Research, Computational and Information Systems Laboratory, Boulder, CO. https://doi.org/https://doi.org/10.5065/D65Q4T4Z.

NCL. (2018). The NCAR Command Language (Version 6.5.0) [Software]. https://doi.org/http://dx.doi.org/10.5065/D6WD3XH5

Nicholson, S. E. (1986). The spatial coherence of African Rainfall Anomalies: interhemispheric Teleconnection. American Meteorological Society.

Nicholson, S. E. (2014). The Predictability of Rainfall over the Greater Horn of Africa. Part I: Prediction of Seasonal Rainfall. *Journal of Hydrometeorology*, *15*(3), 1011–1027. https://doi.org/10.1175/JHM-D-13-062.1

Nicholson, S. E. (2015). The Predictability of Rainfall over the Greater Horn of Africa. Part II: Prediction of Monthly Rainfall during the Long Rains. *Journal of Hydrometeorology*, *16*(5), 2001–2012. https://doi.org/10.1175/JHM-D-14-0138.1

Nicholson, S. E. (2018). The ITCZ and the Seasonal Cycle over Equatorial Africa. *Bulletin of the American Meteorological Society*, *99*(2), 337–348. https://doi.org/10.1175/BAMS-D-16-0287.1

Nijssen, B., O'Donnell, G. M., Lettenmaier, D. P., Lohmann, D., & Wood, E. F. (2001). Predicting the discharge of global rivers. *Journal of Climate*, *14*(15), 3307–3323. https://doi.org/10.1175/1520-0442(2001)014<3307:PTDOGR>2.0.CO;2

NMA. (2018). National Meteorological Agency: Hydro-meteorological Bulletin., 24.

Noble, E., Druyan, L. M., Fulakeza, M., Noble, E., Druyan, L. M., & Fulakeza, M. (2017). The Sensitivity of WRF Daily Summertime Simulations over West Africa to Alternative Parameterizations. Part II: Precipitation. *Monthly Weather Review*, *145*(1), 215–233. https://doi.org/10.1175/MWR-D-15-0294.1

Ntwali, D., Ogwang, B. A., & Ongoma, V. (2016). The Impacts of Topography on Spatial and Temporal Rainfall Distribution over Rwanda Based on WRF Model. *Atmospheric and Climate Sciences*, *06*(02), 145–157. https://doi.org/10.4236/acs.2016.62013

Olaniyan, E., Adefisan, E. A., Oni, F., Afiesimama, E., Balogun, A. A., & Lawal, K. A. (2018). Evaluation of the ECMWF Sub-seasonal to Seasonal Precipitation Forecasts during the Peak of West Africa

Monsoon in Nigeria. *Frontiers in Environmental Science*, *6*, 4. https://doi.org/10.3389/fenvs.2018.00004

Otieno, G., Mutemi, J., Opijah, F., Ogallo, L., & Omondi, H. (2018). The Impact of Cumulus Parameterization on Rainfall Simulations over East Africa. *Atmospheric and Climate Sciences*, *08*(03), 355–371. https://doi.org/10.4236/acs.2018.83024

Palmer, T. N., Shutts, G. J., Hagedorn, R., Doblas-Reyes, F. J., Jung, T., & Leutbecher, M. (2005). REPRESENTING MODEL UNCERTAINTY IN WEATHER AND CLIMATE PREDICTION. *Annu. Rev. Earth Planet. Sci*, *33*, 163–193. https://doi.org/10.1146/annurev.earth.33.092203.122552

Parker, D. J., Priest, S. J., & Tapsell, S. M. (2008). Seasonal forecasting of Ethiopian Spring rains. *Meteorological Applications*, *15*(January), 73–83. https://doi.org/10.1002/met

Pérez, J. C., Díaz, J. P., González, A., Expósito, J., Rivera-López, F., & Taima, D. (2014). Evaluation of WRF Parameterizations for Dynamical Downscaling in the Canary Islands. *Journal of Climate*, *27*(14), 5611–5631. https://doi.org/10.1175/JCLI-D-13-00458.1

Pohl, B., Crétat, J., & Camberlin, P. (2011). Testing WRF capability in simulating the atmospheric water cycle over Equatorial East Africa. *Climate Dynamics*, *37*(7–8), 1357–1379. https://doi.org/10.1007/s00382-011-1024-2

Powers, J. G., Klemp, J. B., Skamarock, W. C., Davis, C. A., Dudhia, J., Gill, D. O., … Duda, M. G. (2017). The Weather Research and Forecasting Model: Overview, System Efforts, and Future Directions. *Bulletin of the American Meteorological Society*, *98*(8), 1717–1737. https://doi.org/10.1175/BAMS-D-15-00308.1

Quitián-Hernández, L., Fernández-González, S., González-Alemán, J. J., Valero, F., & Martín, M. L. (2018). Analysis of sensitivity to different parameterization schemes for a subtropical cyclone. *Atmospheric Research*, *204*, 21–36. https://doi.org/10.1016/J.ATMOSRES.2018.01.001

Ramarohetra, J., Pohl, B., & Sultan, B. (2015). Errors and uncertainties introduced by a regional climate model in climate impact assessments: example of crop yield simulations in West Africa. *Environmental Research Letters*, *10*(12), 124014. https://doi.org/10.1088/1748-9326/10/12/124014

Ratna, S. B., Ratnam, J. V., Behera, S. K., Rautenbach, C. J. d. W., Ndarana, T., Takahashi, K., & Yamagata, T. (2014). Performance assessment of three convective parameterization schemes in WRF for downscaling summer rainfall over South Africa. *Climate Dynamics*, *42*(11–12), 2931–2953. https://doi.org/10.1007/s00382-013-1918-2

Res, C., Ratnam, J. V, Behera, S. S. K., Krishnan, R., Doi, T., & Ratna, S. B. S. (2017). Sensitivity of Indian summer monsoon simulation to physical parameterization schemes in the WRF model. *Climate Research*, *74*(1), 43–66. https://doi.org/10.3354/cr01484

Reynolds, R. W., & Chelton, D. B. (2010). Comparisons of Daily Sea Surface Temperature Analyses for 2007–08. *Journal of Climate*, *23*(13), 3545–3562. https://doi.org/10.1175/2010JCLI3294.1

Reynolds, R. W., Rayner, N. A., Smith, T. M., Stokes, D. C., & Wang, W. (2002). An Improved In Situ and Satellite SST Analysis for Climate. Retrieved December 20, 2018, from https://iridl.ldeo.columbia.edu/SOURCES/.NOAA/.NCEP/.EMC/.CMB/.GLOBAL/.Reyn_SmithOIv2/.monthly/.sst/index.html?Set-Language=en

Robertson, A. W., & Tippett, M. K. (2017). Multimodel Ensembling of Subseasonal Precipitation Forecasts over North America. *Monthly Weather Review*, *145*(October), 16. https://doi.org/10.1175/MWR-D-17-0092.1

Rowell, D. P. (2013). Simulating SST Teleconnections to Africa: What is the State of the Art? *Journal of Climate*, *26*(15), 5397–5418. https://doi.org/10.1175/JCLI-D-12-00761.1

Saha, S., Moorthi, S., Wu, X., Wang, J., Nadiga, S., Tripp, P., … Becker, E. (2011). CEP Climate Forecast System Version 2 (CFSv2) 6-hourly Products. Research Data Archive at the National Center for Atmospheric Research, Computational and Information Systems Laboratory. *Journal of Climate*, *27*(6), 2185–2208. https://doi.org/https://doi.org/10.5065/D61C1TXF

Saha, S., Moorthi, S., Wu, X., Wang, J., Nadiga, S., Tripp, P., … Becker, E. (2014). The NCEP Climate Forecast System Version 2. *Journal of Climate*, *27*(6), 2185–2208. https://doi.org/10.1175/JCLI-D-12-00823.1

Sampson, K., & Gochis, D. (2018). *WRF Hydro GIS Pre-Processing Tools, Version 5.0 Documentation*. Retrieved from https://ral.ucar.edu/sites/default/files/public/WRFHydro_GIS_Preprocessor_v5.pdf

Sathiyamoorthy, V., Pal, P. K., & Joshi, P. C. (2007). Intraseasonal variability of the Tropical Easterly Jet. *Meteorol Atmos Phys*, *96*, 305–316. https://doi.org/10.1007/s00703-006-0214-7

Schepen, A., Wang, Q. J., & Robertson, D. E. (2012). Combining the strengths of statistical and dynamical modelling approaches for forecasting Australian seasonal rainfall. *Journal of Geophysical Research Atmospheres*, *117*(20), 1–9. https://doi.org/10.1029/2012JD018011

Segele, Z. T., & Lamb, P. J. (2005). Characterization and variability of Kiremt rainy season over Ethiopia. *Meteorol Atmos Phys*, *89*, 153–180. https://doi.org/10.1007/s00703-005-0127-x

Segele, Z. T., Lamb, P. J., & Leslie, L. M. (2009). Seasonal-to-Interannual Variability of Ethiopia/Horn of Africa Monsoon. Part I: Associations of Wavelet-Filtered Large-Scale Atmospheric Circulation and Global Sea Surface Temperature. *Journal of Climate*, *22*(12), 3396–3421. https://doi.org/10.1175/2008JCLI2859.1

Segele, Z. T., Richman, M. B., Leslie, L. M., & Lamb, P. J. (2015). Seasonal-to-Interannual Variability of Ethiopia/Horn of Africa Monsoon. Part II: Statistical Multimodel Ensemble Rainfall Predictions. *Journal of Climate*, *28*(9), 3511–3536. https://doi.org/10.1175/JCLI-D-14-00476.1

Seleshi, Y., & Zanke, U. (2004). Recent changes in rainfall and rainy days in Ethiopia. *International Journal of Climatology*, *24*(8), 973–983. https://doi.org/10.1002/joc.1052

Senatore, A., Mendicino, G., Gochis, D. J., Yu, W., Yates, D. N., & Kunstmann, H. (2015). Fully coupled atmosphere-hydrology simulations for the central Mediterranean: Impact of enhanced hydrological parameterization for short and long time scales, *7*, 1693–1715. https://doi.org/10.1002/2015MS000510

Senatore, A., Mendicino, G., Knoche, H. R., Kunstmann, H., Senatore, A., Mendicino, G., … Kunstmann, H. (2014). Sensitivity of Modeled Precipitation to Sea Surface Temperature in Regions with Complex Topography and Coastlines: A Case Study for the Mediterranean. *Journal of Hydrometeorology*, *15*(6), 2370–2396. https://doi.org/10.1175/JHM-D-13-089.1

Shanko, D., & Camberlin, P. (1998). The effects of the southwest Indian ocean tropical cyclones on Ethiopian drought. *International Journal of Climatology*, *18*(12), 1373–1388. https://doi.org/10.1002/(SICI)1097-0088(1998100)18:12<1373::AID-JOC313>3.0.CO;2-K

Siddique, R., Mejia, A., Brown, J., Reed, S., & Ahnert, P. (2015). Verification of precipitation forecasts from two numerical weather prediction models in the Middle Atlantic Region of the USA: A precursory analysis to hydrologic forecasting. *Journal of Hydrology*, *529*, 1390–1406. https://doi.org/10.1016/j.jhydrol.2015.08.042

Siegmund, J., Bliefernicht, J., Laux, P., & Kunstmann, H. (2015a). Toward a seasonal precipitation prediction system for West Africa : Performance of CFSv2 and high-resolution dynamical downscaling. https://doi.org/10.1002/2014JD022692.Received

Siegmund, J., Bliefernicht, J., Laux, P., & Kunstmann, H. (2015b). Towards a Seasonal Precipitation Prediction System for West Africa: Performance of CFSv2 and High Resolution Dynamical Downscaling. *J. Geophys. Res. Atmos.*, 2014JD022692+. https://doi.org/10.1002/2014jd022692

Silver, M., Karnieli, A., Ginat, H., Meiri, E., & Fredj, E. (2017). An innovative method for determining hydrological calibration parameters for the WRF-Hydro model in arid regions. *Environmental Modelling and Software*, *91*, 47–69. https://doi.org/10.1016/j.envsoft.2017.01.010

Simon, J. M. (2008). *From dynamical model predictions, (chapter in Seasonal Climate: Forecasting and Managing Risk.* (S. J. M. Alberto Troccoli, Mike Harrison, David L.T.Anderson, Ed.) (NATO Science). Gallipoli, Italy: Springer. Retrieved from http://www.nato.int/science

Sittichok, K., Djibo, A. G., Seidou, O., Saley, H. M., Karambiri, H., & Paturel, J. (2016). Statistical seasonal rainfall and streamflow forecasting for the Sirba watershed, West Africa, using sea-surface temperatures. *Hydrological Sciences Journal*, *61*(5), 805–815. https://doi.org/10.1080/02626667.2014.944526

Skamarock, C., Klemp, B., Dudhia, J., Gill, O., Barker, D., Duda, G., … Powers, G. (2008). A Description of the Advanced Research WRF Version 3. https://doi.org/10.5065/D68S4MVH

Slingo, J., & Palmer, T. (2011). Uncertainty in weather and climate prediction. *Philosophical Transactions. Series A, Mathematical, Physical, and Engineering Sciences*, *369*(1956), 4751–4767. https://doi.org/10.1098/rsta.2011.0161

Song, Q., Chelton, D. B., Esbensen, S. K., Thum, N., & O'neill, L. W. (2009). Coupling between Sea Surface Temperature and Low-Level Winds in Mesoscale Numerical Models. J*OURNAL OF CLIMATE*, *22*. https://doi.org/10.1175/2008JCLI2488.1

Srivastava, P. K., Han, D., Rico-Ramirez, M. A., Neill, P. O., Islam, T., Gupta, M., … Dai, Q. (2015). Performance evaluation of WRF-Noah Land surface model estimated soil moisture for hydrological application: Synergistic evaluation using SMOS retrieved soil moisture. *Journal of Hydrology*, *529*(P1), 200–212. https://doi.org/10.1016/j.jhydrol.2015.07.041

Stensrud, D. J. (2007). *Parameterization Schemes: Keys to Understanding Numerical Weather Prediction Models*. Cambridge: Cambridge University Press. https://doi.org/10.1017/CBO9780511812590

Stephanie, G., Noel, S. K., Teferi, D., D., Francois, C., Yiguo, W., & Ellen, V. (2017). Seasonal predictability of Kiremt rainfall in coupled general circulation models. *Environmental Research Letters*, *12*(IOP Publishing), 114016. https://doi.org/https://doi.org/10.1088/1748-9326/aa8cfa

Stevens, B., Giorgetta, M., Esch, M., Mauritsen, T., Crueger, T., Rast, S., … Roeckner, E. (2013). Atmospheric component of the MPI-M Earth System Model: ECHAM6. *Journal of Advances in Modeling Earth Systems*, *5*(2), 146–172. https://doi.org/10.1002/jame.20015

Stockdale, T., Johnson, S., Ferranti, L., Balmaseda, M., & Briceag, S. (2018). ECMWF's new long-range forecasting system SEAS5. *ECMWF Newsletter*, *154*(154), 15–20. https://doi.org/10.21957/tsb6n1

Tang, J., Niu, X., Wang, S., Gao, H., Wang, X., & Wu, J. (2016). Statistical downscaling and dynamical downscaling of regional climate in China: Present climate evaluations and future climate projections. *Journal of Geophysical Research: Atmospheres*, *121*(5), 2110–2129. https://doi.org/10.1002/2015JD023977.Received

Taylor, K. E. (2001). Summarizing multiple aspects of model performance in a single diagram. *Journal of Geophysical Research: Atmospheres*, *106*(D7), 7183–7192. https://doi.org/10.1029/2000JD900719

Tian, D., Wood, E. F., & Yuan, X. (2017). CFSv2-based sub-seasonal precipitation and temperature forecast skill over the contiguous United States. *Hydrol. Earth Syst. Sci*, *21*, 1477–1490. https://doi.org/10.5194/hess-21-1477-2017

TigrayTV. (2018a). Ethiopian local media: Tigrai TV Morning News August 2018 - YouTube. Retrieved from https://www.youtube.com/watch?v=EvsY_yvg1xc

TigrayTV. (2018b). Ethiopian local media: Tigrai TV morning news September 15, 2018 - YouTube. *Tigary TV*. Retrieved from https://www.youtube.com/watch?v=mOw-jEg04N8

Vecchi, G. A., Zhao, M., Wang, H., Villarini, G., Rosati, A., Kumar, A., … Gudgel, R. (2011). Statistical–Dynamical Predictions of Seasonal North Atlantic Hurricane Activity. *Monthly Weather Review*, *139*(4), 1070–1082. https://doi.org/10.1175/2010MWR3499.1

Verri, G., Pinardi, N., Gochis, D., Tribbia, J., Navarra, A., Coppini, G., & Vukicevic, T. (2017). A meteo-hydrological modelling system for the reconstruction of river runoff: The case of the Ofanto river catchment. *Natural Hazards and Earth System Sciences*, *17*(10), 1741–1761. https://doi.org/10.5194/nhess-17-1741-2017

Villarini, G., & Serinaldi, F. (2012). Development of statistical models for at-site probabilistic seasonal rainfall forecast. *International Journal of Climatology*, *32*(14), 2197–2212. https://doi.org/10.1002/joc.3393

Vitart, F, Balsamo, G, Buizza, R, Ferranti, L, Keeley, S, Magnusson, L, Molteni, F, Weisheimer, A. (2014). *Sub-seasonal predictions | ECMWF*. *ECMWF*. Retrieved from https://www.ecmwf.int/en/elibrary/12943-sub-seasonal-predictions

Vitart, F., Medium, F., Weather, R., Robertson, A. W., Frédéric, V., Andrew, W. R., & David, L. T. A. (2012). Subseasonal to Seasonal Prediction Project: bridging the gap between weather and climate. *WMO Bulletin 61 (2)*, (June 2014). Retrieved from http://www.wmo.int/pages/prog/arep/wwrp/new/documents/

Vitart, F., & Robertson, A. W. (2018). PERSPECTIVE The sub-seasonal to seasonal prediction project (S2S) and the prediction of extreme events. *Npj Climate and Atmospheric Science*, *1*, 3. https://doi.org/10.1038/s41612-018-0013-0

Wang, Q. J., Schepen, A., & Robertson, D. E. (2012). Merging seasonal rainfall forecasts from multiple statistical models through Bayesian model averaging. *Journal of Climate*, *25*(16), 5524–5537. https://doi.org/10.1175/JCLI-D-11-00386.1

Warner, T. T. (2011). *Numerical Weather and Climate Prediction*. Cambridge University Press. https://doi.org/10.1017/CBO9780511763243

White, C. J., Carlsen, H., Robertson, A. W., Klein, R. J. T., Lazo, J. K., Kumar, A., … Zebiak, S. E. (2017). Potential applications of subseasonal-to-seasonal (S2S) predictions. *Meteorological Applications*, *24*(3), 315–325. https://doi.org/10.1002/met.1654

Wilby, R. L., Wedgbrow, C. S., & Fox, H. R. (2004). Seasonal predictability of the summer hydrometeorology of the River Thames, UK. *Journal of Hydrology*, *295*(1–4), 1–16. https://doi.org/10.1016/j.jhydrol.2004.02.015

Wilks, D. S., & Vannitsem, S. (2018). Uncertain Forecasts From Deterministic Dynamics. *Statistical Postprocessing of Ensemble Forecasts*, *3*, 1–13. https://doi.org/10.1016/B978-0-12-812372-

0.00001-7

WMO. (2018). Weather | World Meteorological Organization. Retrieved September 10, 2018, from https://public.wmo.int/en/our-mandate/weather

Wood, A. W., Leung, L. R., Sridhar, V., & Lettenmaier, D. P. (2004). *HYDROLOGIC IMPLICATIONS OF DYNAMICAL AND STATISTICAL APPROACHES TO DOWNSCALING CLIMATE MODEL OUTPUTS*. Retrieved from https://link.springer.com/content/pdf/10.1023%2FB%3ACLIM.0000013685.99609.9e.pdf

Yao, R., Agyeman, K., Annor, T., Lamptey, B., Quansah, E., Agyekum, J., … Tieku, S. A. (2017). Optimal Physics Parameterization Scheme Combination of the Weather Research and Forecasting Model for Seasonal Precipitation Simulation over Ghana. *Advances in Meteorology*, *2017*. https://doi.org/10.1155/2017/7505321

Yucel, I., Onen, A., Yilmaz, K. K., & Gochis, D. J. (2015). Calibration and evaluation of a flood forecasting system: Utility of numerical weather prediction model, data assimilation and satellite-based rainfall. *Journal of Hydrology*, *523*, 49–66. https://doi.org/10.1016/j.jhydrol.2015.01.042

Zabel, F., & Mauser, W. (2013). 2-way coupling the hydrological land surface model PROMET with the regional climate model MM5. *Hydrology and Earth System Sciences*, *17*(5), 1705–1714. https://doi.org/10.5194/hess-17-1705-2013

Zaitchik, B. F. (2017). Madden-Julian Oscillation impacts on tropical African precipitation. *Atmospheric Research*, *184*, 88–102. https://doi.org/10.1016/j.atmosres.2016.10.002

Zajaczkowski, F. J., Haupt, S. E., & Schmehl, K. J. (2011). A preliminary study of assimilating numerical weather prediction data into computational fluid dynamics models for wind prediction. *Journal of Wind Engineering and Industrial Aerodynamics*, *99*(4), 320–329. https://doi.org/10.1016/j.jweia.2011.01.023

Zaroug, M. A. H., Giorgi, F., Coppola, E., Abdo, G. M., & Eltahir, E. A. B. (2014). Simulating the connections of ENSO and the rainfall regime of East Africa and the upper Blue Nile region using a climate model of the Tropics. *Hydrology and Earth System Sciences*, *18*(11), 4311–4323. https://doi.org/10.5194/hess-18-4311-2014

Zeleke, T., Giorgi, F., Mengistu Tsidu, G., & Diro, G. T. (2013). Spatial and temporal variability of summer rainfall over Ethiopia from observations and a regional climate model experiment. *Theoretical and Applied Climatology*, *111*(3–4), 665–681. https://doi.org/10.1007/s00704-012-0700-4

Zeleke, T. T., Giorgi, F., Diro, G. T., & Zaitchik, B. F. (2017). Trend and periodicity of drought over Ethiopia. *International Journal of Climatology*, *37*(13), 4733–4748. https://doi.org/10.1002/joc.5122

Zinyengere, N., Mhizha, T., Mashonjowa, E., Chipindu, B., Geerts, S., & Raes, D. (2011). Using seasonal climate forecasts to improve maize production decision support in Zimbabwe. *Agricultural and Forest Meteorology*, *151*(12), 1792–1799. Retrieved from https://www.sciencedirect.com/science/article/pii/S0168192311002504

8. Appendix

8.1.1 Pearson's moment correlation coefficient

For continuous time series pairs (Y_t, X_t) variables, the Pearson's moment correlation coefficient will be calculated as;

$$Cor\ (Y_t, X_t) = \frac{\sum_{t=1}^{n}(\mathrm{Y}_t - \overline{\mathrm{Y}})\ (\mathrm{X}_t - \overline{\mathrm{X}})}{\sigma\mathrm{Y} * \sigma\mathrm{X}} \ldots\ldots\ldots\ldots\ldots (Equ\ 8.1)$$

Where t isa time series of n sample size$(\mathrm{t} = 1, 2, 3, \ldots, \mathrm{n})$, σY and σX are the standard deviations of the $Y_t\ and\ X_t$ and $\overline{\mathrm{Y}}$ and $\overline{\mathrm{X}}$ are the mean values of the $Y_t\ and\ X_t$ variables , respectively. The ocean-atmospheric variables that show close to 1 or -1 correlation value indicate strong dependency.

8.2 Statistical methods

8.2.1 Multiple linear regression

For continuous time series data with i^{th} sample series, and n sample size *(i.e., i= 1, 2, 3,…, n)*, if the rainfall (predictand) response *(P_i)* is depending on the oceanic-atmospheric changes of the SST anomalies (SST_{ij} , where *j* represents oceanic regions, *j= I,2, 3, ..., n*) and the zonal winds (U_{ik}, where k is zonal wind levels, k= 1, 2, 3,…, n), the relationship will be developed using a multiple linear regression model as;

$$P_i = \beta_1\ SST_{ij} + \ \beta_2 u_{ij} + \varepsilon \ldots\ldots\ldots\ldots\ldots\ldots\ldots\ldots (Equ. 8.2)$$

Where β_1 and β_2 are the regression coefficients, and ε is the error.

8.2.2 Accuracy measures

The accuracy of the regression model in relation to the in-situ observation values will be evaluated using Root Mean Square Error (RMSE), Mean Absolute Error (MAE) and Bias (Mean Error). This measures the difference between model simulations and in-situ observations and will be calculated using Equ. 8.4 for MAE, Equ.8.5 for RMSE and Equ.8.3 for the Bias (ME). RMSE estimates the average squared difference between the forecasts and observation which helps to determine the systematic and random error. While the Mean Error (ME) measures the difference between the model-simulated and observed rainfall due to systematic errors. A zero or closes to zero value of these statistical methods indicate the perfection or good accuracy of the statistical model.

$$ME = Bias = \frac{1}{n}\sum_{i=1}^{n}(Obs_t - Sim_t) = \ \ldots\ldots\ldots\ldots (Equ. 8.3)$$

$$MAE = \frac{1}{n}\sum_{t=1}^{n}|Obs_t - Sim_t| \ldots\ldots\ldots\ldots\ldots\ldots\ldots\ldots (Equ. 8.4)$$

$$RMSE = \sqrt{\frac{1}{n}\sum_{t=1}^{n}(Obs_t - Sim_t)^2} \ \ldots\ldots\ldots\ldots\ldots\ldots\ldots (Equ. 8.5)$$

8.2.3 The Skill Score (SS) techniques

The SS indicates how the model improves the forecast skill in relative to the reference forecast. In continuous variable, the term reference forecast usually states the climatology or persistence (Warner, 2011). In this study, the skill score (SS) of the prediction models will be estimated using the Mean Square Error (MSE: Warner, 2011) as it is given by *Equ.8.6*.

$$SS = \left(1 - \frac{MSE}{MSE_{ref}}\right) * 100 \ldots\ldots\ldots\ldots\ldots\ldots\ldots\ldots\ldots\ldots (Equ. 8.6)$$

Where the MSE is estimated as;

$$MSE = \frac{1}{n}\sum_{t=1}^{n}(Obs_t - Sim_t)^2 \ldots\ldots\ldots\ldots\ldots\ldots\ldots\ldots (equa. 8.7)$$

$$MSE_{clim} = MSE_{ref} = \frac{1}{n}\sum_{t=1}^{n}(\overline{X} - Obs_t)^2 \ldots\ldots\ldots\ldots (Equ.\ 8.8)$$

Where $\overline{X}$ is the climatological mean of the observed rainfall (X) of the area and the SS value close to zero indicates no improvement on the foresting skill.

8.2.4 Nash-Sutcliffe Efficiency (NSE)

The NSE coefficient provides normalized indicators of the goodness-of-test of hydrological models. It measures the accuracy of the model outputs (mainly runoff and soil moisture) in relation to in-situ observations (Naabil et al., 2017). For a minimal acceptance of hydrometeorological models, the NSE value should be between 0 to 1.0 and the threshold value of NSE that indicates sufficient prediction skill of the WRF-Hydro model should be between [0.5, 0.65].

$$NSE = \frac{\sum_{t=1}^{T}(Q_{sim}^{t} - Q_{ob}^{t})^2}{\sum_{t=1}^{T}(Q_{ob}^{t} - \overline{Q_{ob}})^2} \ldots\ldots\ldots\ldots\ldots (Equ. 8.9)$$

Where Q_{ob}^{t} and Q_{sim}^{t} are observed and model simulated river flows at a time series *t,* respectively.

8.2.5 Taylor diagram

In this study, the Taylor diagrams (Taylor, 2001) will be employed to visualize the strength and weakens of different model parameters and configurations in reproducing the observed values. The diagram will present the RMSE, correlation and standard deviation between the model simulated and observations in a single window on a 2-D polar coordinates plot. This diagram may suggest the optimal model parameters and also provides the errors due to the limitations of different configurations (Abdelwares et al., 2017; Andrys et al., 2015; Hoedjes et al., 2014; Iguchi et al., 2017; Li et al., 2014; Noble et al., 2017).